

# The uncertain future of mountaintop-removal-mined landscapes 2: Modeling the influence of topography and vegetation

Samuel J. Bower<sup>a</sup>, Charles M. Shobe<sup>a,b</sup>, Aaron E. Maxwell<sup>a</sup>, Benjamin Campforts<sup>c</sup>

<sup>a</sup>*Department of Geology and Geography, West Virginia University, Morgantown, WV, USA*

<sup>b</sup>*Now at: United States Forest Service, Rocky Mountain Research Station, Fort Collins, CO, USA*

<sup>c</sup>*Department of Earth Sciences, Vrije University, Amsterdam, Netherlands*

---

---

SJB: [sjb00020@mix.wvu.edu](mailto:sjb00020@mix.wvu.edu)

CMS: [charles.shobe@usda.gov](mailto:charles.shobe@usda.gov) (corresponding author)

AEM: [aaron.maxwell@mail.wvu.edu](mailto:aaron.maxwell@mail.wvu.edu)

BC: [b.campforts@vu.nl](mailto:b.campforts@vu.nl)

---

---

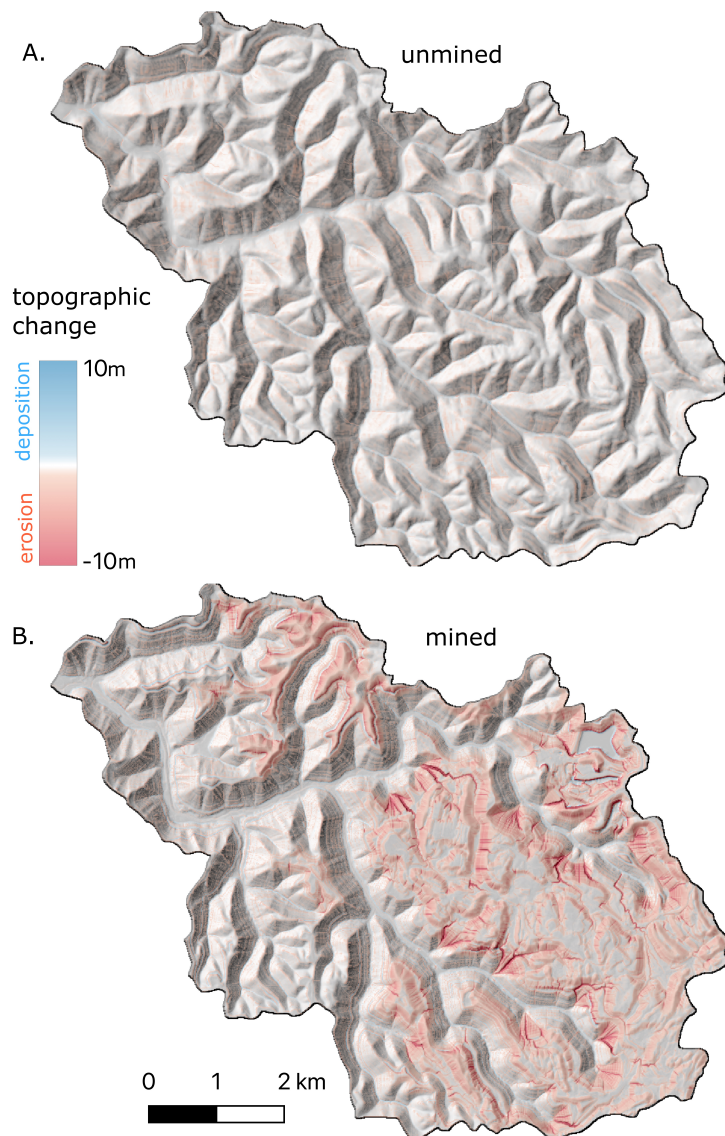
This EarthArXiv preprint has been resubmitted to *Geomorphology* after one round of peer review but has NOT yet been accepted. Subsequent versions of the manuscript may differ from this one. If accepted, the final, published version of this manuscript will be available via a link on this webpage. Please feel free to contact the corresponding author with questions and/or feedback.

1 Graphical Abstract

2 **The uncertain future of mountaintop-removal-mined landscapes 2:**

3 **Modeling the influence of topography and vegetation**

4 Samuel J. Bower, Charles M. Shobe, Aaron E. Maxwell, Benjamin Campforts





5 Highlights

6 **The uncertain future of mountaintop-removal-mined landscapes 2:**  
7 **Modeling the influence of topography and vegetation**

8 Samuel J. Bower, Charles M. Shobe, Aaron E. Maxwell, Benjamin Campforts

- 9     • We model 10,000 years of erosion beginning from both pre- and post-  
10       mining topography.
- 11     • Mining-driven topographic changes alone reduce total erosion due to  
12       ridge flattening.
- 13     • Incomplete vegetation recovery increases erosion in mined over unmined  
14       basins.
- 15     • Erosion is focused in valley fills, deposition in low-order valleys and  
16       below scarps.
- 17     • Vegetation recovery sets decadal sediment pulses and millennial land-  
18       scape trajectory.

19 The uncertain future of mountaintop-removal-mined  
20 landscapes 2: Modeling the influence of topography and  
21 vegetation

22 Samuel J. Bower<sup>a</sup>, Charles M. Shobe<sup>a,b,\*</sup>, Aaron E. Maxwell<sup>a</sup>, Benjamin  
23 Campforts<sup>c</sup>

*<sup>a</sup>Department of Geology and Geography, West Virginia  
University, Morgantown, WV, USA*

*<sup>b</sup>Now at: United States Forest Service, Rocky Mountain Research Station, Fort  
Collins, CO, USA*

*<sup>c</sup>Department of Earth Sciences, Vrije University, Amsterdam, Netherlands*

---

24 **Abstract**

25 Erosion following human disturbance threatens ecosystem health and inhibits  
26 effective land use. Mountaintop removal/valley fill (MTR/VF) mined land-  
27 scapes of the Appalachian Coalfields region, USA, provide a unique opportu-  
28 nity to quantify the geomorphic trajectory of disturbed lands. Here we assess  
29 how MTR/VF-induced changes to topography and vegetation influence spa-  
30 tiotemporal erosion patterns in five mined watersheds. We use landscape  
31 evolution models starting from pre- and post-MTR/VF topographic data to  
32 isolate the influence of mining-induced topographic change. We then con-  
33 strain ranges of erodibility from incision depths of gully features on mine  
34 margins, and use those estimates to model the influence of vegetation recov-  
35 ery trends on erosion.

36 Topographic alterations alone reduce total sediment export from mined  
37 catchments. Model runs that incorporate the disturbance and recovery of  
38 vegetation in mined watersheds show that complete vegetation recovery keeps

39 millennial sediment export from mined catchments within the range of un-  
40 mined catchments. If vegetation recovery is anything less than complete, veg-  
41 etation disturbance drives greater total sediment export from mined catch-  
42 ments than unmined catchments. Full vegetation recovery causes sediment  
43 fluxes to decline over millennia beyond the recovery period, while those with-  
44 out full recovery experience fluxes that increase over the same time period.  
45 Spatiotemporal erosion trends depend on 1) the extent of vegetation recov-  
46 ery and 2) the extent to which MTR/VF creates slope–area disequilibrium.  
47 Valley fills and mine scarps experience erosion rates several times higher than  
48 those found in the unmined landscapes. Rapid erosion of mined areas drives  
49 deposition in colluvial hollows, headwater stream valleys, and below scarps.  
50 Our experiments suggest that reclamation focused on maximizing vegetation  
51 recovery and reducing hotspots of slope–area disequilibrium would reduce  
52 MTR’s influence on Appalachian watersheds both during and long after the  
53 vegetation recovery period. Insights from MTR/VF-influenced landscapes  
54 can inform mined land management as the renewable energy transition drives  
55 increased surface mining.

56 *Keywords:* Post-mining erosion, Landscape evolution, Appalachia,  
57 Reclamation, Erosion prediction

---

## 58 **1. Introduction**

59 Human-induced rates of earth-moving outpace natural rates by upwards  
60 of an order of magnitude (Hooke, 2000; Wilkinson, 2005; Dethier et al., 2022).  
61 Understanding present and future dynamics of landscape evolution requires  
62 the study of Earth’s surface as a coupled natural-human system (Pelletier

63 et al., 2015).

64 One of the most significant contributors to anthropogenic earth-moving  
65 and subsequent landscape change is surface mining—the extraction of ma-  
66 terial by stripping of overburden from above. Some of the highest rates of  
67 mass redistribution in the contiguous United States, for example, are found  
68 in the Appalachian Coalfields (AC) region (Hooke, 1999), despite relatively  
69 low geological erosion rates in this area (Gallen, 2018). This discrepancy is  
70 caused by widespread surface coal mining (e.g., Skousen and Zipper, 2021),  
71 a process of mass redistribution several orders of magnitude more efficient  
72 than background geologic processes (Hooke, 1999). The impending renew-  
73 able energy transition promises to usher in a global acceleration in earth  
74 moving through surface mining due to increased demand for critical min-  
75 erals (Vidal et al., 2013; Sonter et al., 2018; Sovacool et al., 2020; Shobe,  
76 2022). Studying how post-mining landscapes evolve is therefore essential to  
77 minimizing geomorphological and environmental disturbances (e.g., Hancock  
78 et al., 2020a).

79 The AC region provides a particularly instructive case study in post-  
80 mining landscape change because of the sheer magnitude of topographic  
81 rearrangement driven by mountaintop removal/valley fill (MTR/VF) min-  
82 ing, a region-specific type of surface mining where, rather than bench cut-  
83 ting along contours, the entirety of the rock mass above a horizontal coal  
84 seam is blasted/scraped off (Skousen and Zipper, 2021). Waste rock is then  
85 packed and terraced in headwater valleys—resulting in landforms known as  
86 valley fills—to lower the risk of slope failure and prevent erosion (Michael  
87 et al., 2010). The resulting landscape is geomorphically novel in the sense

88 that it contains configurations of landforms that would not develop through  
89 landscape self-organization (Reed and Kite, 2020; Jaeger and Ross, 2021).  
90 Because MTR/VF landscapes are not self-formed, they are likely to expe-  
91 rience unnatural trajectories of post-mining landscape evolution, leading to  
92 undesirable geomorphological and environmental outcomes. Developing the  
93 ability to predict how MTR/VF-mined landscapes evolve once mining and  
94 reclamation are complete will allow improved protection of ecosystems and  
95 water resources, and will provide a useful case study that can be applied to  
96 improve management of mined lands globally.

97 Numerical forward modeling of landscape evolution provides a framework  
98 for predicting how mass redistribution will modify landscapes in the future  
99 (e.g., Tucker and Hancock, 2010; Barnhart et al., 2020b; Hancock and Willgo-  
100 ose, 2021; Kwang et al., 2023). Landscape evolution models have already en-  
101 abled extensive geomorphic prediction and hypothesis testing in post-mining  
102 landscapes (e.g., Willgoose and Riley, 1998; Lowry et al., 2013; Hancock et al.,  
103 2000, 2015). While static, empirical soil erosion models (i.e., RUSLE) have  
104 been used to assess the short-term geomorphic effects of MTR/VF mining  
105 (Sears et al., 2020), there have been no long-term process-based studies of  
106 the geomorphic response to MTR/VF mining in the AC region.

107 In this study we seek to understand how post-MTR/VF landscapes evolve  
108 and how their trajectories of landscape evolution differ from unmined land-  
109 scapes. To do this we leverage a unique dataset consisting of pre- and post-  
110 mining digital elevation models (DEMs) of five watersheds in the AC region.  
111 MTR/VF mining in the AC presents us with an unnatural experiment (cf.  
112 Tucker, 2009) that we can use to directly compare landscape evolution dy-

113 namics between unmined watersheds, which were captured in the pre-mining  
114 DEM but no longer exist, and mined watersheds. We explore two influ-  
115 ences of MTR/VF mining on subsequent landscape evolution: alterations  
116 to topography driven by mining-induced mass redistribution and changes to  
117 land-surface erodibility caused by the loss, and potential subsequent recovery,  
118 of forest cover on mined lands. Our goals are to quantify:

- 119 1. Differences between pre- and post-mining landscape evolution driven  
120 by mining-induced topographic change alone, and
- 121 2. The sensitivity of post-mining landscape change to the extent of vege-  
122 tation recovery.

123 The current study follows from our companion paper (Shobe et al., in  
124 review), which identifies how MTR/VF mining changes geomorphic processes  
125 and variables. Here we quantify how those changes influence post-mining  
126 landscape evolution.

## 127 **2. Background: Post-MTR/VF landscape evolution**

128 MTR/VF mining leaves behind landscapes that are significantly altered  
129 from their natural state. Our companion paper (Shobe et al., in review) an-  
130 alyzes these modifications in detail; here we summarize the key changes in-  
131 duced by MTR/VF that might influence future landscape change. MTR/VF  
132 alters topography, land-surface hydrology, vegetation, and surface and sub-  
133 surface material properties. These changes lead to erosion process dynamics  
134 that differ between mined and unmined landscapes.

135 MTR/VF mining flattens ridgetops and fills headwater river valleys with  
136 waste rock, creating plateau-like landscapes that cover tens of square kilo-

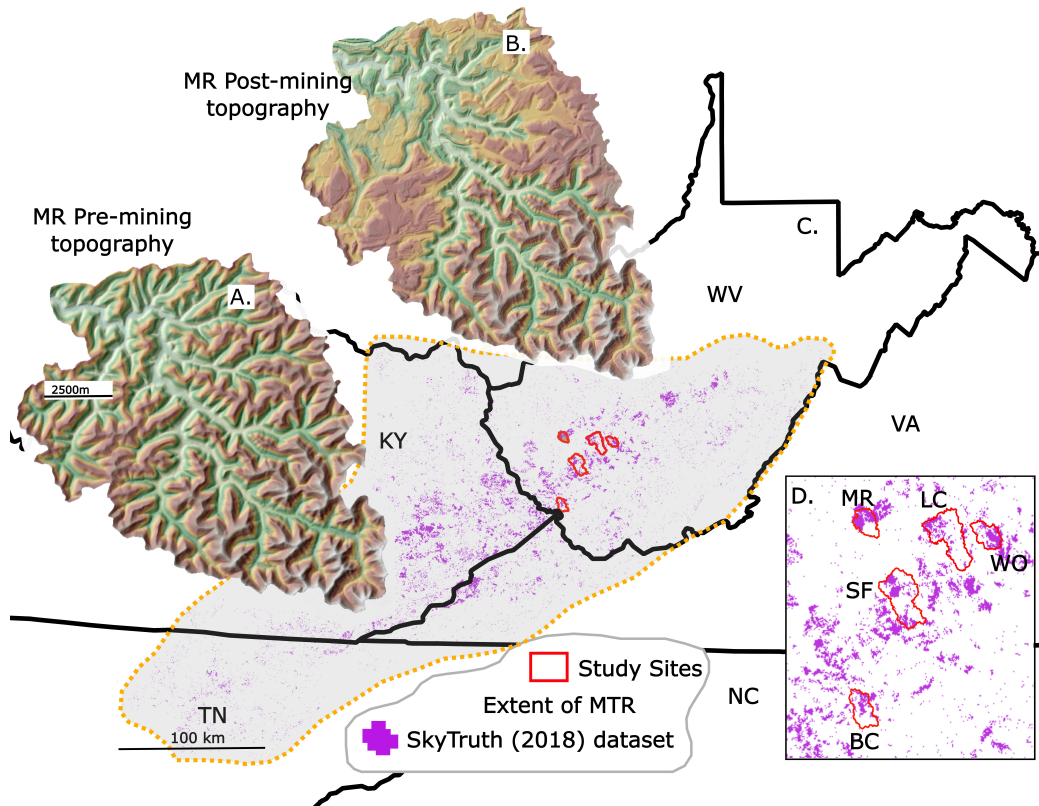


Figure 1: Study region overview. The extent of MTR/VF is approximated by the grey polygon encompassing the purple regions, which are areas mapped as mined from 1985–2015 Landsat imagery (Pericak et al., 2018). Insets A and B show the pre-mining and post-mining DEMs of the Mud River watershed. Panel D zooms in to the five study watersheds. BC: Ben Creek, LC: Laurel Creek, MR: Mud River, SF: Spruce Fork, WO: White Oak.

137 meters (Fig. 1; Ross et al., 2016). These effects are prevalent throughout the  
 138 AC region; mined areas cover  $>5,900 \text{ km}^2$  of land area in the AC (Pericak  
 139 et al., 2018). Valley fills had buried  $>2,000 \text{ km}$  of headwater streams by  
 140 2002 (Bernhardt and Palmer, 2011; EPA, 2011); the current number is not  
 141 known but must be greater due to ongoing MTR/VF mining. The cutting



142 and filling method of MTR/VF causes meaningful alterations to watershed  
143 elevation, slope, and drainage area distributions (Maxwell and Strager, 2013;  
144 Ross et al., 2016; Jaeger and Ross, 2021; Shobe et al., in review). MTR/VF  
145 mining creates large areas of the landscape with near-zero slopes where moun-  
146 taintops have been removed, as well as new steeply sloping areas where valley  
147 fills in headwater valleys end and grade steeply down to the old valley bot-  
148 tom (Ross et al., 2016; Jaeger and Ross, 2021). Average catchment elevation,  
149 slope, and slope–area product are significantly, monotonically correlated with  
150 the percent of a catchment that has undergone MTR/VF mining—positively,  
151 negatively, and negatively, respectively (Shobe et al., in review). MTR/VF  
152 also dramatically rearranges drainage divides, reallocating flow among wa-  
153 tersheds (Shobe et al., in review).

154 The impact of MTR/VF on surface and groundwater hydrology is com-  
155 plex due to variations among reclamation techniques and individual MTR/VF  
156 landforms (Phillips, 2004; Miller and Zégre, 2014; Nippgen et al., 2017; Shobe  
157 et al., in review). Changes in topography (primarily slope reduction) and the  
158 de-vegetation of large portions of drainage basins influence surface hydrology,  
159 as do mining-induced changes to the water balance and flow routing.  
160 Across the mined landscape in general, infiltration rates tend to be lower  
161 than for unmined areas for the first few years post-mining (e.g., Guebert and  
162 Gardner, 2001). Cut surfaces—areas where mass has been removed—tend to  
163 have lower infiltration rates than filled areas, because in cut areas bedrock  
164 is close to the surface while filled areas are underlain by tens of meters of  
165 fractured mine spoil. This duality accounts for field observations suggest-  
166 ing that though high volumes of runoff might be generated from the cut

167 portions of mined landscapes (Negley and Eshleman, 2006) and drive local  
168 erosion hotspots (Reed and Kite, 2020), the larger-scale catchment hydrology  
169 of mined basins often shows higher baseflows and less stormflow than nearby  
170 unmined basins (Nippgen et al., 2017).

171 MTR/VF causes changes to vegetation and subsequent recovery trends  
172 that create permanently altered ecological conditions. Reclamation regula-  
173 tions mandate post-mining planting, but do not require restoration to the  
174 original forested state—regulations allow landowners to select vegetation re-  
175 covery plans to accommodate desired land use (Bell et al., 1989; Skousen and  
176 Zipper, 2014). Remote-sensing-derived indices of vegetation recovery indicate  
177 that mine sites that attempted reforestation have not in general experienced  
178 the return of mature forests. Proxies for vegetation recovery tend to, over  
179 the decades since reclamation, asymptotically approach values that are sub-  
180 optimal relative to undisturbed ecosystems (Ross et al., 2021; Thomas et al.,  
181 2022). A reasonable rule of thumb for post-mining forest recovery, given the  
182 inherent complexity in succession dynamics and the limitation of remotely  
183 sensed vegetation proxies, is to say that it recovers towards the pre-mining  
184 condition but that it may never recover fully.

185 MTR/VF also dramatically alters surface and subsurface material prop-  
186 erties. Once mining ceases, the mined area is resurfaced with minesoil, which  
187 can be soil that is stockpiled from the pre-mining landscape, brought in from  
188 elsewhere, or constructed by crushing waste rock (Bell et al., 1989). Beneath  
189 the few cm to tens of cm of minesoil, there can exist intact bedrock (cut  
190 areas) or deep piles of highly heterogeneous waste rock (filled areas). Both  
191 minesoils and the waste rock that can underlie them are highly heteroge-

192 neous. Minesoils often exhibit grain size distributions that are overall finer  
193 than native soils, but with a disproportionately large coarse fraction (Feng  
194 et al., 2019). Valley fill deposits typically have a framework of large boul-  
195 ders at the base overlain by highly variable sand- to boulder-sized fill (e.g.,  
196 Michael et al., 2010; Greer et al., 2017). Though geotechnical properties of  
197 minesoils and underlying fill vary widely, mined landscapes likely have less  
198 near-surface cohesion than their natural counterparts due to the combination  
199 of vegetation loss and physical heterogeneity (Shobe et al., in review).

200 Changes to topography, hydrology, vegetation, and material properties  
201 cause unique erosion dynamics on post-MTR/VF landscapes. Investigations  
202 of slope–area relationship in mined watersheds show shifts towards fluvial  
203 erosion in portions of slope–area space where hillslope processes once dom-  
204 inated (Jaeger and Ross, 2021). These process changes manifest in mined  
205 landscapes as deeply incised gullies on the peripheries of mined areas (Reed  
206 and Kite, 2020).

207 While there are no studies forecasting how changes driven by MTR/VF  
208 mining might integrate to influence post-MTR/VF landscape evolution, we  
209 can draw general insights from other regions and types of mines. An extensive  
210 body of work centered around the evolution of spoil piles and other landforms  
211 on Australian uranium mines has yielded insight into how mined landscapes  
212 might evolve. In these settings, landscape evolution is dominated by rapid  
213 gully erosion that moves sediment quickly during and after mining (Hancock  
214 et al., 2000, 2015; Hancock and Willgoose, 2021). Modeling studies suggest  
215 that vegetation (Evans and Willgoose, 2000; Hancock et al., 2015; Lowry  
216 et al., 2019), precipitation (Hancock et al., 2017b,a; Lowry et al., 2019), and

217 grain size (Lowry et al., 2019; Hancock et al., 2020b) all have significant  
218 impacts on sediment flux over annual timescales and catchment hypsometry  
219 over geologic timescales (Hancock et al., 2016). Most important in controlling  
220 the trajectory of landscape change is the shape of the engineered post-mining  
221 landscape, which governs the distribution of slope and drainage area (e.g.,  
222 Lowry et al., 2019; Hancock et al., 2020a; Jaeger and Ross, 2021).

223 In this study we seek to gain similar insight into the evolution of post-  
224 MTR/VF landscapes. We model the effects of two of the four key modifica-  
225 tions to post-MTR/VF landscapes: topography and vegetation. Though we  
226 suspect that alterations to hydrology and surface material properties are also  
227 important (Shobe et al., in review), these influences are less well quantified  
228 than changes to topography (revealed by DEMs; Maxwell and Strager, 2013;  
229 Ross et al., 2016; Jaeger and Ross, 2021) and vegetation (revealed by spectral  
230 metrics; Ross et al., 2021; Thomas et al., 2022).

### 231 **3. Methods**

232 We seek to elucidate the influence of 1) topographic alteration and 2)  
233 vegetation (non-)recovery on post-MTR/VF landscape evolution through nu-  
234 merical landscape evolution experiments using pre- and post-mining DEMs.

#### 235 *3.1. Experimental design*

236 We model landscape evolution over the next 10 kyr for five heavily mined  
237 watersheds in the AC region. For each watershed, we conduct a control  
238 simulation in which landscape evolution begins from the pre-mining DEM  
239 and we assume no changes to geomorphic processes or variables. Control  
240 simulations reveal the trajectory of landscape change the watershed would

241 have experienced had it not been mined or subjected to any other major  
242 disturbance.

243 To isolate the influence of MTR/VF-driven topographic change, we con-  
244 duct a simulation for each watershed using the post-mining DEM under the  
245 simplifying assumption that nothing has changed due to mining except the  
246 watershed’s topography. We do not suggest that mined landscapes experi-  
247 ence no other alterations (see Shobe et al., in review), only that comparing  
248 these results with the results of the unmined simulations allows us to isolate  
249 the influence of topographic change.

250 We then explore how the recovery, or lack thereof, of vegetation influences  
251 post-mining landscape evolution. We do this by manipulating the erodibil-  
252 ity of the land surface under the assumption that more mature vegetation  
253 communities (i.e., forest) reduce erodibility by increasing soil cohesion. We  
254 simulate three vegetation recovery scenarios (Sec. 3.4.1) for each watershed:  
255 one in which vegetation (and therefore erodibility) does not recover at all  
256 post-mining, one in which vegetation recovers to its pre-mining state, and  
257 one where vegetation recovery returns erodibility half of the way to its pre-  
258 mining value.

259 Our experimental design results in five forward models of landscape change  
260 in each study watershed: one based on the pre-mining topography, one in  
261 which only topography has been influenced by mining, and three explor-  
262 ing the sensitivity of post-mining landscape evolution to vegetation-related  
263 erodibility changes. We do not investigate changes to hydrology and material  
264 properties (e.g., Shobe et al., in review) in this initial analysis.

HUC-12 ID	Name	A [km <sup>2</sup> ]	Pre-R [m]	Post-R [m]	% mined
050702010302	Ben Creek	60	524	521	25
050500090602	Laurel Creek	130	478	458	22
050701020302	Mud River	50	280	280	38
050500090302	Spruce Fork	130	500	477	20
050500090601	White Oak	50	513	467	31

Table 1: The five study watersheds. A is catchment area, Pre-R is pre-mining topographic relief, and Post-R is post-mining topographic relief. Percent mined values are calculated from landsat-derived mining extents (Pericak et al., 2018).

### 265 3.2. Study watersheds

266 This study uses five hydrologic unit code 12 (HUC-12) catchments from  
267 the AC region (Fig. 1). These watersheds are representative of mined water-  
268 sheds in the AC in that they display high relief and steep hillslopes driven  
269 by river incision that outpaces lithologically controlled ridgetop lowering.  
270 We focus on these five watersheds because their pre- and post-mining geo-  
271 morphology was quantified and characterized in detail by Jaeger and Ross  
272 (2021). Study watersheds range from 50 to 130 km<sup>2</sup> in area and have all  
273 experienced MTR/VF mining over at least 20% of their surface area (Ta-  
274 ble 1); this has dramatically rearranged their topography (DEMs in Fig. 1).  
275 We note that because MTR/VF rearranges drainage divides (Shobe et al., in  
276 review), watershed boundaries do not remain the same between the pre- and  
277 post- mining cases. Given that we have to keep our analysis area consistent,  
278 however, we use the HUC-12 watershed boundaries for both cases.

279 MTR/VF mining has meaningfully changed the topography of all five  
280 catchments (Figs. 1 and 2; Jaeger and Ross (2021); Shobe et al. (in review)).

281 Mining has narrowed their elevation distributions as peaks are flattened and  
282 valleys are filled (Fig. 2A–E). Slope distributions become bimodal with in-  
283 creasing proportions of low slopes that represent flattened areas (Fig. 2F–J).  
284 Distributions of the slope–area product ( $\sqrt{AS}$ , a proxy for the efficacy of  
285 erosion by flowing water; e.g., Howard and Kerby, 1983) show increasing  
286 proportions of the landscape underlain by areas of low  $\sqrt{AS}$ , both because  
287 slopes are reduced in general and because headwater valleys have been re-  
288 placed with flat regions in which flow does not accumulate as efficiently with  
289 distance (Fig. 2K–O). Bayesian Wilcoxon signed-rank tests (van Doorn et al.,  
290 2020) comparing pre- and post-mining distributions suggest that all three to-  
291 pographic metrics are significantly different between the pre- and post-mining  
292 DEMs of all five watersheds (Fig. 2). The pre- and post-MTR/VF topog-  
293 raphy for each catchment will serve as initial conditions in the modeling  
294 study and allow for quantitative comparison between erosion of disturbed  
295 landscapes and their now-lost natural counterparts.

### 296 *3.3. Numerical modeling approach*

297 We model sediment erosion, transport, and deposition on pre- and post-  
298 mining DEMs over the next 10 kyr. Our modeling approach errs on the  
299 side of simplicity, attempting to incorporate environmental complexity where  
300 we have the data to do so while avoiding unconstrained complexity. This  
301 requires making major simplifications to the treatment of surface hydrology  
302 and landscape material properties, the implications of which we discuss in  
303 Sec. 5.4.

304 To capture erosion by overland flow, we use the Stream Power with Al-  
305 luvium Conservation and Entrainment (SPACE) model (Shobe et al., 2017)



306 in the Landlab modeling toolkit (Barnhart et al., 2020a). Hillslope sediment  
 307 transport by creep and heave processes is modeled using a linear diffusion  
 308 equation (e.g., Culling, 1963).

309 The model treats elevation change over time  $\frac{\partial z}{\partial t}$  [m/yr] as the sum of  
 310 fluvial and hillslope processes:

$$\frac{\partial z}{\partial t} = U + \frac{D_s - E_s}{1 - \phi} + D\nabla^2 z, \quad (1)$$

311 where  $U$  [m/yr] is rock uplift relative to baselevel,  $D_s$  and  $E_s$  are volumetric  
 312 rates per unit bed area of sediment deposition and entrainment [m/yr], re-  
 313 spectively,  $\phi$  is bed sediment porosity [-], and  $D$  is the efficiency of hillslope  
 314 sediment transport [m<sup>2</sup>/yr].

315 Our formulation excludes the bedrock erosion term commonly incorpo-  
 316 rated in the SPACE model, making it equivalent to the erosion–deposition  
 317 model of Davy and Lague (2009). While we acknowledge that bedrock lies  
 318 near the surface in portions of both unmined and mined AC landscapes, we  
 319 do not have 1) adequate constraints on depth to bedrock across our study  
 320 watersheds or 2) a way to establish reasonable bounds on bedrock erodibility.  
 321 By neglecting bedrock erosion we are implicitly assuming that AC bedrock  
 322 has similar erodibility to overlying sediment, which may or may not be true  
 323 at any given location but is not an unreasonable starting assumption given  
 324 the heterogeneity in both AC bedrock and in unmined and post-mining AC  
 325 soils.

326 The volumetric sediment entrainment rate per unit bed area  $E_s$  is

$$E_s = K(x, t) (AP)^{0.5} S^n, \quad (2)$$

327 where  $K(x, t)$  [ $\text{m}^{-0.5}\text{yr}^{-0.5}$ ] is the erodibility of surface material which we vary  
 328 as a parameter in space and time,  $A$  is drainage area [ $\text{m}^2$ ],  $P$  is mean an-  
 329 nual precipitation (MAP) [ $\text{m}/\text{yr}$ ],  $S$  is surface slope, and  $n$  is a slope expo-  
 330 nent. There is no limitation placed on entrainment rate by sediment (un-  
 331 )availability (Shobe et al., 2017) because we do not distinguish between sed-  
 332 iment and bedrock. Eq. 2 encapsulates our two most significant model sim-  
 333 plifications: the assumption that erosion by flowing water is set by drainage  
 334 area, local slope, and MAP, and the assumption that both cut and filled  
 335 portions of MTR/VF landscapes exhibit similar material properties.

336 The volumetric sediment deposition rate per unit bed area  $D_s$  is

$$D_s = \frac{Q_s}{Q}V, \quad (3)$$

337 where  $Q_s$  is volumetric sediment flux [ $\text{m}^3/\text{yr}$ ],  $Q$  is volumetric water discharge  
 338 [ $\text{m}^3/\text{yr}$ ] and  $V$  is the effective sediment settling velocity [ $\text{m}/\text{yr}$ ] (Davy and  
 339 Lague, 2009).

340 We use D8 flow routing with the Priority Flood algorithm (Barnes, 2017),  
 341 which routes flow across depressions in the landscape. This is important on  
 342 MTR/VF landscapes where there are many flat regions and engineered de-  
 343 pressions (Reed and Kite, 2020; Shobe et al., in review). Our approach as-  
 344 sumes that runoff is generated equally across the landscape, though there are  
 345 probably differences in hydrologic response between cut and filled portions  
 346 of mined areas (Nippgen et al., 2017; Shobe et al., in review).

### 347 3.4. *Constraining parameter values*

348 The model contains several parameters, some of which we treat as steady  
 349 and uniform and some of which are unsteady and/or nonuniform. Sediment

350 porosity  $\phi$  is fixed at 0.3 and the slope exponent  $n$  at 1. The efficiency  
351 of hillslope sediment transport  $D$  is treated as steady and uniform with a  
352 value of 0.003 m<sup>2</sup>/yr, taken from a recent global compilation that includes  
353 the Appalachians (Richardson et al., 2019). A major assumption we make is  
354 that the efficiency of hillslope sediment transport does not vary between un-  
355 mined and mined landscapes. While this is not likely to be strictly true given  
356 the differences in material properties between unmined and mined areas and  
357 observed landslides in valley fills (Reed and Kite, 2020), erosion by flowing  
358 water is thought to be the dominant erosion mechanism on MTR/VF land-  
359 scapes (Reed and Kite, 2020; Jaeger and Ross, 2021). Further, given that  
360 our timescale of interest is only 10 kyr, the efficiency of hillslope transport is  
361 unlikely to exert a first-order control on landscape evolution (e.g., Barnhart  
362 et al., 2020b). So while we likely miss second-order details of the system by  
363 keeping hillslope transport efficiency constant, changes to AC hillslope pro-  
364 cesses driven by mining are probably not as important as changes to fluvial  
365 incision processes.

#### 366 *3.4.1. Fluvial erodibility and the influence of vegetation recovery*

367 Gully incision by flowing water is thought to be the dominant agent of  
368 post-MTR/VF landscape evolution (Reed and Kite, 2020; Jaeger and Ross,  
369 2021), so quantitatively constraining the fluvial erodibility constant  $K$  is  
370 paramount. MTR/VF-induced changes to erodibility are poorly understood,  
371 but likely result from altered near-surface material properties as well as the  
372 deforestation that accompanies mining (Shobe et al., in review). Following  
373 the conceptual model from our companion paper (Shobe et al., in review,  
374 their Fig. 11), we make the simplifying assumption that the revegetation

375 trajectory of mined landscapes controls the evolution of erodibility through  
376 time. Increased vegetation cover and root density on mined lands likely  
377 has a variety of erosion-inhibiting effects (Shobe et al., in review) ranging  
378 from reducing overland flow volumes by increasing evapotranspiration (e.g.,  
379 Nippgen et al., 2017) to increasing soil cohesion (e.g., Simon and Collison,  
380 2002). We might therefore expect erodibility to be highest immediately post-  
381 reclamation when mines are planted with grasses or small saplings. Erodi-  
382 bility might then decrease over reforestation timescales as succession occurs.  
383 Though revegetation does occur to some extent, the consensus is that forests  
384 do not return to their pre-mining state over the multidecadal timescales for  
385 which we have observations (e.g., Wickham et al., 2013; Ross et al., 2021;  
386 Thomas et al., 2022).

387 We constrain the range of  $K$  on MTR/VF-mined landscapes by mapping  
388 gullies from lidar data (Fig. 3) and using gully morphology and erosion rates  
389 to calculate  $K$  (Fig. 4). We assume, based on past field observations (Reed  
390 and Kite, 2020; Jaeger and Ross, 2021), that gullies on post-mine landforms  
391 are features that post-date mining because deeply incised gullies are not  
392 commonly observed in natural Appalachian landscapes. Constraining  $K$  by  
393 mapping erosional features allows us to assess the integrated effects of changes  
394 to surface material properties, vegetation, and the erosivity of overland flow  
395 (for example due to changes in storm hydrographs), influences which we do  
396 not have the data to tease apart individually.

397 We measured the average depths, slopes, and drainage areas of 176 gullies  
398 from our five MTR/VF-mined watersheds using 2018 lidar (1 m resolution;  
399 Fig. 3 shows an example). Each gully was assigned a minimum age based on

400 the last year that the mine complex hosting the gully was mapped as actively  
 401 mined in the Landsat-derived dataset of Pericak et al. (2018). Dividing gully  
 402 depth by minimum age yields a maximum incision rate (Fig. 4). There is  
 403 no clear relationship between gully incision rates and slope or drainage area,  
 404 which suggests that variability in erosion rates might arise from mining-  
 405 induced variations in land-surface erodibility. We use these gully incision  
 406 rates along with their drainage area and slope to calculate a distribution of  
 407  $K$  within mined landscapes by rearranging the simple, detachment-limited  
 408 form of the stream power incision model:

$$\frac{\partial z}{\partial t_{\text{obs}}} = -K_{\text{calc}} A^{0.5} S, \quad (4)$$

409 where  $\frac{\partial z}{\partial t_{\text{obs}}}$  is the observed erosion rate (and is negative to indicate land-  
 410 surface lowering),  $A$  is drainage area, and  $S$  is slope, to yield the inferred  
 411 erodibility  $K_{\text{calc}}$ :

$$K_{\text{calc}} = \frac{-\frac{\partial z}{\partial t_{\text{obs}}}}{A^{0.5} S}. \quad (5)$$

412 We find an over two order of magnitude range in  $K_{\text{calc}}$  (Fig. 4). We take  
 413 the median of the  $K_{\text{calc}}$  distribution to indicate the maximum extent to which  
 414 erodibility can be perturbed by mining, thereby incorporating the bulk of our  
 415 data while avoiding possible outliers (Fig. 4).

416 Because our methodology relies on mapping post-mining erosion features  
 417 to calculate  $K$ , it cannot produce estimates of  $K$  for unmined Appalachian  
 418 landscapes. Geologic-timescale estimates of  $K$  for this region come from  
 419 Gallen (2018), who used river profile analysis to find a region-averaged  $K$   
 420 value for the Appalachian Plateau of approximately  $1.3 \times 10^{-6} \text{ m}^{0.1} \text{ yr}^{-1}$ . The

421 0.05 difference in drainage area exponent  $m$  between Gallen (2018)'s analysis  
422 and ours leads to only a 30% change in our calculated ratio of maximum to  
423 minimum post-mining  $K$  values, a minor difference given the uncertainties  
424 in  $m$  and in our procedure for constraining  $K$ . We therefore take  $K$  to be  
425  $1.3 \times 10^{-6} \text{ yr}^{-1}$  for unmined landscapes, then take the ratio between the me-  
426 dian and minimum  $K$  values we infer from gullies on mined lands (Fig. 4) as  
427 representative of the extent to which mining can cause  $K$  to rise above its  
428 natural value. By doing so we implicitly assume that the lowest-erodibility  
429 post-mining landscapes have similar erodibilities to undisturbed landscapes.  
430 We do not have evidence for or against the validity of this assumption, but it  
431 is unavoidable because we do not have independent constraints from compa-  
432 rable methods on how erodibility varies between the least disturbed mined  
433 landscapes and undisturbed ones. We prefer this over the alternative of di-  
434 rectly comparing  $K$  values mapped from decades of post-mining gully erosion  
435 against Gallen (2018)'s background  $K$  estimate that integrates over geologic  
436 time because of the dramatic mismatches in spatial and temporal scale be-  
437 tween the two methods.

438 Our calculated erodibilities, when scaled to the long-term background  
439 erodibility of Gallen (2018), therefore range from a minimum of  $K_{\min} =$   
440  $1.3 \times 10^{-6} \text{ yr}^{-1}$  on unmined landscapes to a maximum of  $K_{\max} = 3.4 \times 10^{-5} \text{ yr}^{-1}$   
441 on mined landscapes that have not yet experienced any vegetation recovery.  
442 We did not incorporate MAP (i.e., use Eq. 2) in our gully incision analysis  
443 because our method yields only rough erodibility estimates and would not  
444 be improved by additional complexity. The difference in the dimensions of  
445  $K$  between Eq. 2 and Eq. 5 is reconciled to first order by the fact that MAP

446 is close to 1 m/yr in all of our study watersheds, but for clarity we note that  
447 the units of  $K$  in the model are formally [ $\text{m}^{-0.5}\text{yr}^{-0.5}$ ] because our simulations  
448 incorporate MAP.

449 We explore the parameter space of vegetation recovery influences on erodi-  
450 bility by simulating three different post-mining erodibility scenarios (Fig. 5).  
451 We choose this exploratory approach because of our currently poor under-  
452 standing of post-mining erodibility (Shobe et al., in review): vegetation re-  
453 covery trajectories depend heavily on management decisions, changes to near-  
454 surface material properties may also influence long-term erodibility, and there  
455 are no known relationships between vegetation recovery and land-surface  
456 erodibility. In each scenario, the erodibility immediately post-mining is the  
457 maximum value we inferred from our gully mapping ( $K_{\max}$ ).  $K$  in each  
458 scenario then declines exponentially over 200 years—a rough timescale for  
459 full post-disturbance regeneration of Appalachian hardwood forests—towards  
460 a value  $K_{\min}^*$ , a minimum value imposed by the effectiveness of forest re-  
461 covery. Our three-scenario analysis comprises a no-recovery case in which  
462  $K_{\min}^* = K_{\max}$ , a full recovery case in which  $K_{\min}^* = K_{\min}$ , meaning that  
463  $K$  declines from  $K_{\max}$  to  $K_{\min}$  over 200 years, and a 50% recovery case in  
464 which  $K_{\min}^* = 0.5K_{\max}$ , such that  $K$  declines from  $K_{\max}$  to 50% of  $K_{\max}$  over  
465 200 years. Figure 5 shows all three recovery scenarios, which are defined  
466 quantitatively by:

$$K_{\min}^* = K_{\max} - [(K_{\max} - K_{\min})P_r] \quad (6)$$

467 where  $P_r$  is the proportion of recovery (i.e.,  $K$  returns  $P_r \times 100\%$  of the  
468 way to its pre-mining value). We assume that  $K$  recovery trajectories over



469 time follow a sublinear power law:

$$K = K_{\max} - \left[ \frac{(K_{\max} - K_{\min}^*)}{200^{0.25}} \right] t^{0.25}. \quad (7)$$

470 Here 200 is the 200 years roughly required for an Appalachian hardwood  
471 forest to recover from a disturbance,  $t$  is time since reclamation, and 0.25  
472 is the exponent on the recovery curve we approximate from remote sensing  
473 vegetation recovery data (Ross et al., 2021; Thomas et al., 2022).

474 Once the 200 year recovery period is over, the  $K$  of mined portions of  
475 the landscape is held constant at  $K_{\min}^*$ . Physically, this means that there  
476 is some limit on the extent to which erodibility can recover that is reached  
477 after 200 years.  $K$  is only affected by mining on areas that Landsat imagery  
478 shows have been mined (Pericak et al., 2018); elsewhere on the landscape we  
479 assume that  $K = K_{\min}$  for all time because there was never any disturbance.  
480 This neglects other human disturbances to the landscape like logging, but  
481 allows us to specifically target the influence of MTR/VF mining.

482 There is uncertainty in Pericak et al. (2018)’s Landsat-based analysis of  
483 mined areas that we use to assign mined versus unmined  $K$  values. We  
484 therefore use a moving window to smooth  $K$  values across the landscape to  
485 account for 1) our lack of certainty about the exact boundary between mined  
486 and unmined areas given that their analysis has 30 m resolution while our  
487 DEMs have 10 m resolution, and 2) potential spillover effects of mining onto  
488 areas mapped as unmined, like for example the development of service roads.  
489 We use a smoothing window of nine DEM cells, or  $90 \times 90$  m, because Pericak  
490 et al. (2018) eliminated all mined areas  $< 9,000 \text{ m}^2$  from their analysis on  
491 the basis of uncertainty and using a nine-cell window means that we are

492 smoothing  $K$  over an area as close to that threshold area as possible.

### 493 3.4.2. *Sediment settling velocity*

494 In our erosion–deposition model, the ratio of sediment erodibility  $K$  to  
495 effective settling velocity  $V$  governs how a landscape evolves.  $V$  is a quan-  
496 tity not equal to measured sediment settling velocity, but related to the  
497 net tendency towards deposition once effects of sediment concentration and  
498 upward-directed fluid forces are accounted for (Davy and Lague, 2009; Shobe  
499 et al., 2017).  $\frac{K}{V} \gg 1$  shifts the system towards detachment-limited behavior  
500 and  $\frac{K}{V} \ll 1$  shifts the system towards transport-limited behavior (Davy and  
501 Lague, 2009; Shobe et al., 2017). We treat  $V$  as an empirical constant that we  
502 infer from landscape characteristics. We use  $V = 0.01$  m/yr because while  
503 field evidence indicates dominance of detachment-limited behavior in our  
504 study landscape (i.e., there is a preponderance of bedrock channels; Jaeger,  
505 2015), there are thin mantles of alluvium in most stream valleys such that  
506 we cannot assume no contribution of transport-limited behavior. Because we  
507 calculated  $K$  values from detachment-limited stream power theory alone, by  
508 necessity implicitly assuming that settling velocity is negligible, we need now  
509 to modify our observed  $K$  values to account for the component of gully slope  
510 induced by settling with our assumed value of  $V = 0.01$  m/yr. Equating  
511 the steady-state form of the detachment-limited stream power model with  
512 the steady-state form of the erosion–deposition model (Shobe et al., 2017)  
513 allows us to transform all observed  $K$  values ( $K_{\text{calc}}$ ) to values for use in our  
514 simulations  $K_{\text{sim}}$  that account for the contribution of sediment deposition:

$$\frac{U}{K_{\text{calc}}A^m} = \frac{UV}{K_{\text{sim}}A^mP} + \frac{U}{K_{\text{sim}}A^m}, \quad (8)$$

515 which simplifies to:

$$K_{\text{sim}} = K_{\text{calc}} \left( \frac{V}{P} + 1 \right). \quad (9)$$

516 These conversions allow us to acknowledge the mixed transport- and  
517 detachment-limited behavior of gullies and streams in our study area without  
518 adding undue model complexity. Whether our particular assumption of the  
519 value of  $V$  is correct or not, this approach allows model parameters to be  
520 constrained without assuming a purely detachment-limited system.

### 521 3.4.3. *Precipitation and the influence of climate change*

522 We set  $P$  for each catchment to be the catchment-averaged MAP. As a  
523 consequence of climate change, historical (or current) precipitation data is  
524 not a reasonable proxy for future precipitation. Previous post-mining studies  
525 have used spatial climate change analogues (Hancock et al., 2017b). However,  
526 recent work suggests that we are entering a regime where future climate in  
527 many locations globally does not have a spatial climate analog because of  
528 the magnitude of expected change (Dahinden et al., 2017). We therefore  
529 use climate projections derived from general circulation models (the NASA  
530 BioClim dataset; Pearson et al., 2014) to represent the future trends within  
531 each watershed. We take the average of BioClim’s MAP product, using a  
532 warming scenario that assumes CO<sub>2</sub> stabilization at 450 ppm, over each of  
533 our study watersheds for 2010–2100. After the first 90 years of simulation  
534 time we hold MAP constant at its 2100 value (e.g., Barnhart et al., 2020b),  
535 reasoning that changes beyond that timeline are unpredictable because they  
536 rest on human choices made over the rest of this century.

537 *3.5. Initial and boundary conditions*

538 All simulations begin from either the pre-mining or post-mining DEMs  
539 of Ross et al. (2016). The pre-mining DEM is derived from historical 10m  
540 USGS contour lines pre-dating 1970. The post-mining DEM is derived from  
541 ground-return lidar data flown in 2010 and resampled to the same cell size  
542 (10 m) as the pre-mining DEM (Ross et al., 2016). There is some inherent  
543 variability between DEMs due to the vastly different data collection methods;  
544 it is negligible compared to the enormous topographic changes caused by  
545 MTR/VF mining.

546 We do not use a spin-up period—an initial period of model time intended  
547 to 1) allow erosion of DEM artefacts and 2) enable the landscape to begin  
548 to equilibrate to the model’s simplified landscape evolution mechanics (e.g.,  
549 Coulthard and Skinner, 2016). In our study, the disequilibrium of the unnat-  
550 ural post-mining landscape with respect to the natural geomorphic processes  
551 that formed the pre-mining landscape is the whole point. Using a spin-up pe-  
552 riod would artificially dampen the influence of MTR/VF-driven topographic  
553 change on post-mining erosion.

554 Each study watershed has no-flux boundary conditions imposed along the  
555 boundary of the drainage with the exception of the outlet node, which uses a  
556 Dirichlet boundary condition in which node elevation lowers at a regionally  
557 representative rock uplift/baselevel lowering rate of 0.027 mm/yr (Gallen,  
558 2018)—the geologically “short” (10 kyr) duration of our study makes this rate  
559 relatively inconsequential. All models run for 10 kyr in half-year timesteps  
560 during the recovery period and one-year timesteps for the remaining time.

561 **4. Results**

562 *4.1. Sediment fluxes from mined and unmined watersheds*

563 Our experiments allow us to isolate the influence of topography by com-  
564 paring erosion between mined and unmined DEMs without incorporating  
565 any change in erodibility, and then to assess the influence of erodibility by  
566 comparing among our different forest recovery scenarios.

567 When vegetation-controlled erodibility is held equal between mined and  
568 unmined landscapes, the total sediment flux from all five watersheds is uni-  
569 versally lower in the mined case than the unmined case (Fig. 7). The total  
570 sediment exported over 10 kyr decreased by 8–26% among our five water-  
571 sheds between model runs using the unmined DEM and the mined DEM.  
572 The two catchments in which sediment export changes least in percentage  
573 terms between the simulations using pre- and post-mining topography are  
574 Laurel Creek (11%) and Spruce Fork (8%), which are the two largest catch-  
575 ments and the two catchments in which mining covers the lowest proportion  
576 of the watershed (22% and 20%, respectively). Similarly, the two catch-  
577 ments that experienced the greatest proportional change in sediment flux  
578 between model runs using the pre- versus post-MTR/VF topography, Mud  
579 River (26%) and White Oak (23%), are the smallest catchments and have  
580 the highest proportions of their area mined (38% and 31%, respectively).

581 Acknowledging the fact that mined portions of the landscape are likely  
582 to be initially more erodible—due to their lack of mature vegetation—than  
583 unmined portions of the landscape complicates the relationship between sed-  
584 iment export from mined catchments and sediment export from their un-  
585 mined counterparts (Fig. 7). In the most optimistic recovery scenario, in

586 which erodibility returns to its unmined value after 200 years, sediment ex-  
587 port is 5-7% greater than the mined control case with no erodibility change  
588 but 4-21% less than the unmined case. The two additional revegetation sce-  
589 narios, in which erodibility recovers 50% of the way towards its unmined  
590 value or does not recover at all, show much greater sediment export from the  
591 mined catchments. The progressive increase in sediment export across the  
592 100%, 50%, and 0% recovery cases is slightly less than linear. In the worst  
593 case (0% recovery) scenario, in which erodibility never declines from its high  
594 post-mining value, sediment export is 365%–888% higher than the mined  
595 case with no erodibility change and 326%–627% higher than the unmined  
596 case.

#### 597 *4.2. Temporal patterns in catchment-averaged erosion*

598 Tracking cumulative sediment export from the study watersheds over the  
599 200 year vegetation recovery timescale (Fig. 8, left column) and the remainder  
600 of the 10 kyr simulation (Fig. 8, right column) illustrates temporal erosion  
601 dynamics. All five watersheds exhibit similar patterns.

602 The unmined case and the mined case with no erodibility change show  
603 the same erosion trajectory over time, with only slightly differing volumes of  
604 erosion at any given time due to the presence/absence of mining-altered to-  
605 pography. The most salient differences between the cases in which erodibility  
606 is perturbed by mining (colored solid lines in Fig. 8) and those in which it  
607 is not (dashed lines in Fig. 8) occur in the first 200 years of the simulations  
608 during the period of forest recovery. At the end of the 200 year recovery  
609 period, the worst-case (0%) vegetation recovery scenario produces 317–742%  
610 greater sediment export than the mined case with no erodibility perturba-

611 tion, and 286–535% greater export than the unmined case. The best-case  
612 (100%) recovery scenario produces 71–156% greater sediment export than  
613 the mined case with no erodibility perturbation, and 58–93% greater export  
614 than the unmined case.

615 Vegetation recovery, or lack thereof, over the first 200 years governs the 10  
616 kyr trajectory of erosion and sediment export (Figs. 8 and 9). The best-case  
617 (100%) recovery scenario exhibits a downward trajectory in sediment export  
618 over time (Fig. 9) that approaches that of the mined case with no erodibility  
619 perturbation; differences in sediment export between the two cases decline  
620 from 71–156% after 200 years to 5–7% after 10 kyr. The 100% recovery  
621 scenario ultimately experiences less sediment export than the unmined case,  
622 with 4–21% less sediment export after 10 kyr than the unmined case despite  
623 having 58–93% greater export after 200 years. Conversely, when there is  
624 partial or no forest recovery, mining-induced increases in sediment export  
625 continue to grow over the full 10 kyr period (Fig. 9). The difference between  
626 the worst-case (0%) recovery scenario and the mined and unmined control  
627 cases increases from 317–742% to 365–888% and 286–535% to 326–627%,  
628 respectively over the 9,800 years after the potential forest recovery period  
629 ends. Across all five watersheds, the mined control case, the unmined control  
630 case, and the 100% recovery case experience sediment fluxes that decline over  
631 time from 200–10,000 yrs (Fig. 9). The 0% and 50% recovery cases, however,  
632 experience increases in sediment flux over the same time period.

### 633 *4.3. Distributions of erosion rates*

634 We assess the variability of erosion in space by plotting histograms of  
635 erosion rates for each catchment and model scenario (Fig. 10). Erosion rates



636 are averages over the 10 kyr of model time; positive rates reflect net lowering  
637 of the landscape and negative rates reflect net deposition.

638 In all five watersheds, the erosion rate distribution is right-skewed to some  
639 extent, such that greater proportions of higher erosion rates than higher  
640 deposition rates are observed. In the unmined case and the mined case  
641 with no erodibility change, time-averaged erosion rates do not exceed 0.6  
642 mm/yr anywhere in the study watersheds. The distribution is broader—  
643 that is, maximum erosion and deposition rates are greater—in the mined  
644 case with no erodibility change than in the unmined case. The distribution  
645 of erosion rates becomes progressively more skewed towards higher erosion  
646 rates as the extent to which the erodibility of mined areas recovers to its pre-  
647 mining state declines. The 100% recovery case exhibits an effectively identical  
648 distribution of 10 kyr average erosion and deposition rates to the mined case  
649 with no erodibility change. In the 0% recovery case, portions of the study  
650 catchments can experience erosion rates up to 3.5 mm/yr—maximum rates  
651 are more than double this value but do not affect enough of the catchment to  
652 be visible on Fig. 10—approximately a six-fold increase from the mined case  
653 with no erodibility change. Deposition rates remain fairly consistent among  
654 all mined cases due to the balancing effects of greater erodibility and greater  
655 sediment fluxes.

#### 656 *4.4. Spatial patterns in erosion rates*

657 Erosion over the 10 kyr model runs is highly variable in space (Figs. 11  
658 and 12 show the 50% recovery case in the White Oak watershed, but results  
659 hold across all five watersheds we investigated). While the magnitudes of  
660 erosion change based on the recovery scenario selected, the spatial patterns

661 in erosion do not. In the unmined DEM (Fig. 11A) and the unmined por-  
662 tions of the mined catchment (Fig. 11B; left side of the DEM), erosion is  
663 fairly minimal (maximum of 6.4 m over 10 kyr; <1 m in most areas), except  
664 in locations where DEM artefacts (for example the mosaicing and contour  
665 digitization artefacts visible in Fig. 12A) or non-MTR/VF human alterations  
666 to the landscape (e.g., dams, roads) have driven minor erosion hotspots.

667 Erosion rates across most of the mined portion of the landscape are low,  
668 with the flattened ridgetop/filled valley topography experiencing <1 m of  
669 erosion on its flat surfaces (Figs. 11B and 12). Predicted erosion is greatest  
670 along the margins of the MTR/VF-mined area, with magnitudes of erosion  
671 exceeding 25 m (maximum of 75.8 m) over the 10 kyr period. The locations of  
672 the most rapid predicted erosion are steep valley fill faces, the scarps defining  
673 the edges of the mined areas (and scarps left by reclamation practices within  
674 mined areas), and the steep hillslopes just downslope of mined flats (Fig. 12).  
675 Predicted deposition can exceed 2 m (maximum of 7.4 m) over 10 kyr, and is  
676 concentrated primarily at the base of steep scarps and in low-order valleys,  
677 with more minor amounts in human-made impoundment structures on the  
678 mined surface (Fig. 12).

679 Combining information from the pre-mining DEM, the post-mining DEM,  
680 and the DEM after 10 kyr of simulated erosion across the three erodibility  
681 scenarios we tested allows us to assess the erosion trajectory of landforms  
682 unique to post-MTR/VF watersheds: valley fill faces (Fig. 13A and C), hill-  
683 slopes adjacent to, but not within, the mined area (Fig. 13B), and a hills-  
684 lope reshaped by mining (Fig. 13D). Each landform experiences progressively  
685 more erosion as the simulated recovery of post-mining erodibility towards its

686 pre-mining state is reduced.

687 The valley fill faces (Fig. 13A and C) experience the anthropogenic addi-  
688 tion of tens of meters of topography through the MTR/VF mining process as  
689 headwater river valleys are transformed into waste rock deposits, followed by  
690 the most erosion of any post-MTR/VF landform. We observe severe gullying  
691 in the two fills in Fig. 13A and C, with incision depths up to approximately 50  
692 m below the post-mining land surface. The peripheral but unmined hillslope  
693 (Fig. 13B) experiences approximately 15 m of erosion by gullying. The al-  
694 tered hillslope (Fig. 13D), which experienced significant (up to 20 m) lowering  
695 of the topography over just a 40-year period through mining and reclamation,  
696 experiences diffusive relaxation of the steep scarp resulting in approximately  
697 five meters of surface lowering at the head of the scarp.

## 698 **5. Discussion**

### 699 *5.1. Topographic and vegetation controls on post-MTR/VF erosion*

700 Our analysis isolates the relative influences of MTR/VF-induced topo-  
701 graphic change and vegetation disturbance under the assumption that veg-  
702 etation influences land-surface erodibility. It also brackets the realm of pos-  
703 sibility for post-mining erosion, ranging from permanently and dramatically  
704 increased erodibility to full recovery of erodibility to its pre-mining state.

705 When quantifying the influence of topography alone, we find that mined  
706 watersheds produce less total sediment over 10 kyr than their unmined coun-  
707 terparts (Fig. 7). This occurs because the flattening of large portions of the  
708 landscape, due to both ridge lowering and valley filling, produces large re-  
709 gions with low slope and relatively low drainage area (Maxwell and Strager,

710 2013; Ross et al., 2016; Jaeger and Ross, 2021; Shobe et al., in review). The  
711 significant proportion of the study watersheds (20–38%; Table 1) made up  
712 of this novel geomorphic unit means that the erosion-inhibiting effects of  
713 flattening outweigh the rapid erosion that occurs around the periphery of  
714 mined regions where flattened areas give way to steep natural or constructed  
715 hillslopes (Figs. 11 and 12; Reed and Kite (2020)) when no mining-induced  
716 erodibility changes are considered.

717 The assumption that MTR/VF does not change land-surface erodibility,  
718 however, is likely not valid (Reed and Kite, 2020; Jaeger and Ross, 2021;  
719 Shobe et al., in review). When we relax this assumption and instead as-  
720 sume that erodibility increases immediately after mining and then declines  
721 over time as vegetation recovers (Fig. 5), we find that mined watersheds in  
722 which erodibility does not recover fully to its pre-mining value export more  
723 sediment over the next 10 kyr (Fig. 7) and experience higher peak erosion  
724 rates (Fig. 10) than their unmined counterparts. Given the maximum and  
725 minimum erodibility values we infer from our analysis of gullies on mined  
726 landscapes (Figs. 3 and 4), we find that even recovery of mined landscape  
727 erodibility 50% of the way to its pre-mining state allows efficient enough ero-  
728 sion that sediment export from mined watersheds far outpaces their unmined  
729 counterparts (Fig. 7). Intriguingly, 100% erodibility recovery results in less  
730 total sediment export from mined than unmined watersheds, indicating that  
731 under these conditions the brief increase in erodibility caused by mining is in-  
732 sufficient to overcome the erosion-reducing effect of slope reduction across the  
733 watershed. There exist no data on the relationship between post-MTR/VF  
734 revegetation and erodibility, or on the extent to which the erodibility once

735 vegetation has recovered might be altered by mining-induced material prop-  
736 erty changes, so we cannot assess the likelihood that mined watersheds in  
737 our study region reach any particular recovery threshold. Because we have  
738 been conservative in defining maximum erodibility as the median derived  
739 from our gully mapping, it is probable that forest recovery would need to  
740 be both very efficient and very complete to prevent mined watersheds from  
741 exporting more sediment than unmined ones.

742 Erosion rates are highest in our mined study watersheds (Fig. 8) for the  
743 first few decades after mining because of complementary ecological and geo-  
744 morphic factors. Forest recovery on reclaimed mines seems to approximate  
745 a sublinear power-law function whereby vegetation recovers quickly at first  
746 and then more slowly as it nears (but never reaches) its natural state (e.g.,  
747 Ross et al., 2021; Thomas et al., 2022). Because we have assumed that  
748 erodibility recovers in tandem with vegetation, the most rapid erosion and  
749 sediment export in our study watersheds occurs in the first century while  
750 erodibility is much greater than both its pre-mining value and the value it  
751 will ultimately reach after vegetation recovers to its maximum possible ex-  
752 tent (i.e., 50% or 100% of the way to its pre-mining state). The occurrence of  
753 peak erosion rates immediately after mining is also driven by geomorphology.  
754 Slopes on human-constructed topographic features are steepest immediately  
755 post-mining, and decline over time as erosion proceeds.

756 We can think of post-MTR/VF regions as a set of steep-edged plateaus  
757 being incised by a resurgent drainage network. In these landscapes, the  
758 relative influence of land-surface erodibility and initial topography govern  
759 whether catchment-averaged erosion rates increase or decline over the first 10

760 kyr of landscape evolution. We observe both cases in which high erodibility  
761 allows rapid expansion and integration of the drainage network, steepening  
762 of previously flattened slopes, and resulting increases in catchment-averaged  
763 erosion rates over time (the 0% and 50% recovery scenarios in Fig. 9), as well  
764 as cases in which low erodibility precludes the expansion of erosion hotspots  
765 over our simulation timescale and causes a decline in catchment-averaged  
766 erosion rates over time (the 100% recovery and control scenarios in Fig. 9).  
767 We posit the existence of a critical restoration threshold, consistent across  
768 all five watersheds, that controls the system state (increasing or decreasing  
769 sediment export over time) and is contingent on the magnitude and duration  
770 of human-driven disturbances (e.g., Phillips, 1997; Phillips and Van Dyke,  
771 2016). Our findings suggest that efficiently returning mined land erodibility  
772 to its pre-mining condition may not only keep fluxes from mined watersheds  
773 within the range observed for unmined catchments (Fig. 7), but also set  
774 mined watersheds on a desirable path of declining sediment flux over time  
775 (Fig. 9). Conversely, failing to return mined lands to near their pre-mining  
776 erodibility may, in addition to causing greater sediment export immediately  
777 post-reclamation, lock in millennia of steadily increasing sediment fluxes.

778 Post-mining topography is a fixed initial condition that imposes a fairly  
779 minor reduction in erosion due to topography alone (Fig. 7), so the extent to  
780 which a post-MTR/VF landscape erodes depends primarily on the extent to  
781 which its erodibility increases above, and fails to decline to, the pre-mining  
782 condition. This control can be conceptualized as the erodibility integrated  
783 over time, a quantity that can be increased by greater mining-driven increases  
784 in initial post-mining erodibility, slower recovery of erodibility towards its

785 post-mining state, and/or a greater erodibility even after recovery is com-  
786 plete due to ineffective revegetation or permanent mining-induced material  
787 property changes (Fig. 5). Our findings are consistent with empirical mod-  
788 eling suggesting that the vegetated state of the post-MTR/VF landscape  
789 governs short-term erosion (Sears et al., 2020), and further points to short-  
790 term vegetation recovery remaining a key control on sediment export over  
791 millennia.

792 Vegetation is not the only control on erodibility in post-MTR/VF land-  
793 scapes. Our modeling effort neglects other altered material properties, such  
794 as the grain size distribution of valley fills (Shobe et al., in review), that  
795 likely set the extent to which post-mining landscapes can recover towards  
796 their pre-mining erodibility.

### 797 *5.2. Processes driving hotspots of post-mining landscape change*

798 The margins of MTR/VF landscapes, where mined areas meet unmined  
799 areas, are the primary hotspots of erosion in our experiments. Erosion  
800 hotspots can arise due to gully erosion in areas of drainage network expansion  
801 or due to efficient hillslope sediment transport along steep scarps.

802 Valley fill faces, the staircase-like topographic elements that delineate the  
803 edges of waste rock deposits filling former stream valleys, erode faster than  
804 anywhere else on the landscape (Figs. 11– 13). This occurs because valley  
805 fills are the portions of the post-MTR/VF landscape that are most out of  
806 slope–area equilibrium: their drainage area tends to remain high because  
807 they occupy the sites of former low-order streams, but the average slope  
808 of valley fill faces can reach nearly 0.5 m/m, several times to an order of  
809 magnitude greater than the slopes of headwater streams in the region. This

810 combination of high slope and drainage area drives rapid erosion in our simu-  
811 lations. Though simple landscape evolution models do not make distinctions  
812 between ephemeral gullies and stable perennial stream channels, we inter-  
813 pret the incision of valley fills to be a gullying process in which the channel  
814 network is effectively re-establishing itself by incising into steep, artificial  
815 hillslopes placed in locations of high drainage area.

816 Outside of valley fills, the hillslopes below mined mountaintops also ex-  
817 perience significant erosion in our models (Figs. 11– 13). Gullies incising  
818 mine-adjacent sideslopes that do not themselves fall within the mined area  
819 are deepest at the top of the slope near the mined area, and become shal-  
820 lower as they grade towards the valley floor. We observe this result because  
821 of our choice to smooth the erodibility across the landscape using a moving  
822 window: erodibility smoothly transitions from its mined value to its unmined  
823 value across a distance of 90 m, or nine grid cells. Enhanced erodibility at  
824 the top of mine-adjacent hillslopes therefore allows efficient gullying, while  
825 lower erodibility at the bottom of the same hillslopes reduces gully incision.

826 Observations of gully incision into valley fills and sideslopes along the  
827 periphery of mined areas in our numerical simulations agree with field ob-  
828 servations from MTR/VF landscapes (Reed and Kite, 2020). Reed and Kite  
829 (2020) found that post-MTR/VF landscapes exhibited high gully densities  
830 along the edges of mined areas—a maximum of five gullies per  $\text{km}^2$  of area  
831 mined—and that up to 25% of the gullies along the margin of a given mine  
832 occurred on valley fills. Though they did not pinpoint a cause for each  
833 gully, Reed and Kite (2020) suggested possible causes of gully formation. On  
834 valley fill faces, gullying likely occurs due to the marked geomorphic disequi-



835 librium of the landform combined with its lack of vegetation and potentially  
836 less erosion-resistant material properties. On undisturbed sideslopes below  
837 mined areas, there are no significant vegetation or material property changes,  
838 and Reed and Kite (2020) suggested that gullying in these areas is driven  
839 by pulses of stormwater runoff from reclaimed mines just upslope. They  
840 noted that some sideslope gullies occur just below retention cells, human-  
841 made structures designed to retard runoff from mined landscapes, suggesting  
842 a hydrologic control on gully incision.

843 In light of field observations, we suggest that our model reasonably cap-  
844 tures the mechanisms driving gullying on valley fills but not on mine-adjacent  
845 sideslopes. Valley fills are mapped as mined areas in our forcing data, so ex-  
846 perience greater erodibility than nearby unmined areas. Increased erodibility  
847 on valley fills, combined with their improbable position in slope–area space,  
848 drives expansion of the drainage network by gullying. Our model does not  
849 capture the mechanisms driving sideslope gullying except in a heuristic way.  
850 We observe sideslope gullying because of the way we smooth transitions in  
851 erodibility between mined and unmined landscapes, while the real driver is  
852 thought to be pulses of stormwater runoff (Reed and Kite, 2020), a forcing  
853 not simulated in our models that simply scale water discharge with drainage  
854 area and MAP and assume steady, uniform flow. To capture these dynamics,  
855 our model would need at minimum spatially variable runoff generation.

856 While the greatest predicted erosion depths occur on valley fills due to  
857 their steep slopes, high drainage areas, and high erodibilities, we also observe  
858 significant erosion and deposition along human-made scarps both within and  
859 along the periphery of mined areas (Figs. 11— 13). Scarp erosion is the

860 only natural means of redistributing mass on mined summit flats, where  
861 drainage networks cannot re-establish themselves except by many millennia  
862 of bedrock-erosion-driven lateral retreat of steep mine margins. Scarp ero-  
863 sion is responsible for the highest quantities of sediment deposition observed  
864 in our study as sediment accumulates along mined flats at the base of scarps.  
865 The extent to which our predictions of scarp erosion and deposition are rea-  
866 sonable depends primarily on the material properties of engineered scarps.  
867 In cases where they are constructed of mine spoil, our predicted along-scarp  
868 erosion and deposition depths may be close to minimum values given that  
869 we did not allow vegetation, or lack thereof, to influence the efficiency of hill-  
870 slope processes. When scarps are cut into bedrock, our estimates are likely  
871 close to maximum possible values. Mined scarps also often tend to fail in  
872 mass-wasting events (Bell et al., 1989), suggesting that the linear diffusion  
873 approximation for hillslope processes approximates the long-term average  
874 result of scarp evolution rather than event-scale erosion dynamics.

875 While our assumption of a mostly detachment-limited landscape ( $V =$   
876  $0.01$  m/yr) ensures that maximum deposition rates are substantially lower  
877 than maximum erosion rates (Fig. 10) and that most eroded sediment is ex-  
878 ported from the watersheds, rapid erosion of the margins of MTR/VF-mined  
879 areas results in net sediment accumulation in colluvial hollows and head-  
880 water river valleys (Fig. 12). The combined effects of efficient gully erosion  
881 along mine margins and hillslope sediment transport down steep hillslopes  
882 and valley fill faces results in sediment supply to headwater valleys that, on  
883 average, exceeds fluvial transport capacity. One implication of this focused  
884 deposition is the potential for increased debris flow activity. MTR/VF min-

885 ing may drive erosion patterns that efficiently load steep, low-order channels  
886 with sediment that could then fail during subsequent storm events. Though  
887 MTR/VF mountaintops themselves are, due to being nearly perfectly flat,  
888 devoid of any debris flow activity (Jaeger and Ross, 2021), MTR/VF may  
889 have the effect of pushing the debris flow process domain into areas of slope-  
890 area space that were previously dominated by fluvial processes. There is  
891 currently no data on the relationship between MTR/VF mining and spa-  
892 tiotemporal patterns of debris flows, but the potential for MTR/VF to shift  
893 debris flow locations and dynamics is worth considering given the prevalence  
894 of debris flows as agents of Appalachian landscape evolution (e.g., Eaton  
895 et al., 2003) and geomorphic hazards (e.g., Wiczorek and Morgan, 2008).

896 Substantial sediment deposition in headwater streams, if model predic-  
897 tions are realized, would contribute to MTR’s well-studied negative impacts  
898 on aquatic ecosystems (e.g., Bernhardt and Palmer, 2011). High sedimen-  
899 tation rates are destructive to the endangered endemic amphibian species  
900 that make central Appalachia a critical biodiversity hotspot (Wiley, 2001).  
901 Further, rapid fluvial aggradation could exacerbate flood hazards already  
902 prevalent across Appalachia. Field evidence, however, is mixed on the extent  
903 to which MTR/VF mining drives sedimentation in headwater streams. Rates  
904 of delivery of fine sediment to channels do seem to be greater in mined areas  
905 relative to unmined areas (Jaeger, 2015; Wiley, 2001), but some observations  
906 show increased bedrock exposure in streams that drain mined areas relative to  
907 those that do not (Jaeger, 2015). It is possible that mining-induced changes  
908 to land-surface hydrology, or explicit treatment of multiple grain sizes, would  
909 need to be added to our model to better capture headwater sediment dynam-

910 ics, but our simulations indicate that there is some risk of ecologically de-  
911 structive sedimentation over the long term in headwater streams that drain  
912 heavily mined areas. Our results do not indicate that sedimentation persists  
913 in second- and third-order streams; transport capacity outcompetes sediment  
914 supply in those channels as unmined areas make up a greater proportion of  
915 upslope area. We emphasize, however, that modeled sedimentation rates and  
916 volumes do not incorporate stochastic sediment supply events like storms and  
917 landslides (DeLisle and Yanites, 2023) and depend heavily on the choice of  
918 the effective settling velocity  $V$ . If transport-limited process dynamics are  
919 found to matter in these streams to a greater extent than we have modeled  
920 (i.e., if  $V \gg 0.01$  m/yr), we should expect more sedimentation than our  
921 current set of results predicts. Exploratory model experiments with  $V = 0.1$   
922 m/yr showed this behavior. The sensitivity of modeled headwater stream  
923 sedimentation to  $V$  is important to explore further because of the deleterious  
924 effects of sedimentation on aquatic ecosystems.

### 925 *5.3. Implications for management*

926 Our results suggest that effective revegetation, defined as near-100% re-  
927 covery to pre-mining erodibility within 200 years, can keep millennial sedi-  
928 ment fluxes from reclaimed MTR/VF mines within the range predicted for  
929 unmined landscapes (Fig. 7), but that pulses of accelerated sediment yield  
930 during revegetation are likely (Fig. 8).

931 The revegetation trajectory of reclaimed mines is critical both because  
932 rapid sediment export from mined watersheds occurs during the initial period  
933 of elevated erodibility and because the success of century-timescale reforesta-  
934 tion affects the trajectory of sediment export many millennia into the future

935 (Fig. 9). Reductions in post-mining erodibility can smooth out initial sedi-  
936 ment pulses over longer time periods, potentially mitigating harm to aquatic  
937 ecosystems, and prevent a system state change (Phillips and Van Dyke, 2016)  
938 that leads to increasing sediment export over millennia. Achieving the re-  
939 quired erodibility reductions involves revegetation targeted at reducing the  
940 maximum (presumably immediately post-mining) erodibility, the recovery  
941 timescale, and the erodibility the landscape reaches after full vegetation re-  
942 covery to the greatest extent possible. Reclamation approaches that target  
943 accelerated restoration of forests (e.g., Zipper et al., 2011) have the poten-  
944 tial to reduce post-mining erosion over annual to decadal timescales, but that  
945 potential remains unstudied.

946 Over millennial timescales, MTR/VF landforms seem to erode back to-  
947 wards their prior, self-organized state. Even our scenarios in which erodi-  
948 bility is not perturbed by mining—an unlikely possibility—show that valley  
949 fill faces are erosion hotspots, an outcome that agrees with field observations  
950 (Reed and Kite, 2020). This suggests that as long as mine reclamation in-  
951 volves building valley fill landforms that have high slope and high drainage  
952 area, flowing water will leverage the resulting geomorphic disequilibrium to  
953 re-establish a drainage network, driving erosion of the valley fill surface that  
954 will outpace that of adjacent natural landforms. Even establishing engi-  
955 neered, armored channels along the margins of valley fills can in some cases  
956 prove ineffective at stopping gullyng (Reed and Kite, 2020; Sears et al.,  
957 2020). Our work speaks to the potential importance of Geomorphic Land-  
958 form Design (e.g., Hancock et al., 2003; Lowry et al., 2013; DePriest et al.,  
959 2015; Hancock et al., 2020a), the practice of building landforms that have

960 slope–area distributions as similar as possible to the pre-mining landscape.  
961 In MTR/VF regions this effectively means reducing the mean slope of valley  
962 fill faces (DePriest et al., 2015).

#### 963 *5.4. Limitations and opportunities*

964 This study contains a number of simplifications and assumptions that  
965 future work on post-MTR/VF landscape evolution might be able to relax.

966 Post-MTR/VF landscapes have complex spatial distributions of material  
967 properties (Shobe et al., in review). In our model we assume that the entire  
968 landscape is underlain by a single material as opposed to distinguishing be-  
969 tween sediment and bedrock (Shobe et al., 2017), but distinguishing among  
970 surface material properties can be a first-order control on model–landscape  
971 fidelity (Barnhart et al., 2020c). We also assume that the only control on the  
972 erodibility of mined areas is the extent of vegetation recovery, such that there  
973 is no change in the erodibility driven purely by changes to surface material  
974 properties. But differences between mine soils at the reclaimed surface, the  
975 crushed waste rock of valley fills, and the natural soil column of adjacent  
976 unmined areas likely influence rates of geomorphic change by both fluvial  
977 and hillslope processes.

978 We neglect processes of hillslope failure in our models. However, field  
979 observations show that valley fills can experience landslides (Reed and Kite,  
980 2020), and debris flows are a common agent of geomorphic change in un-  
981 mined Appalachian landscapes (Wieczorek and Morgan, 2008). Whether  
982 post-MTR/VF landscapes are on average more or less susceptible to hill-  
983 slope failures than their unmined counterparts, a more complete model of  
984 post-mining landscape change would include stochastic sediment supply pro-

985 cesses and their interactions with the fluvial system (e.g., Campforts et al.,  
986 2022; DeLisle and Yanites, 2023).

987 The most significant simplifications in our modeling effort relate to land-  
988 surface hydrology. We assumed spatially uniform generation of overland  
989 flow by asserting that fluvial erosion is proportional to upstream area and  
990 MAP. However, most field evidence points toward post-MTR/VF landscapes  
991 having three unique hydrologic domains: cut areas that efficiently generate  
992 overland flow because thin soils overlie less permeable bedrock, filled areas  
993 that efficiently absorb large quantities of water and act as subsurface reser-  
994 voirs, and unmined areas that exhibit intermediate behavior (Nippgen et al.,  
995 2017; Shobe et al., in review). Distinguishing among these three domains  
996 by setting different effective runoff rates or by more detailed simulation of  
997 the water balance might improve the match between predicted and observed  
998 erosion hotspots.

999 We also assume steady, uniform overland flow through the use of a stream-  
1000 power-type model. Reed and Kite (2020) suggested that much of the gully  
1001 erosion occurring on the periphery on mined areas occurs due to overtopping  
1002 of, or intentional discharge from, stormwater retention cells. If the timing  
1003 and location of most post-mining erosion is driven by the spatiotemporal dis-  
1004 tribution of pulses of peak flow, more complex treatments of hydrology and  
1005 hydraulics that include 1) spatial variability in runoff generation, 2) unsteady  
1006 flow, and 3) erosion thresholds, will produce more realistic predictions (e.g.,  
1007 Barnhart et al., 2020c). It also might be worth exploring the interplay be-  
1008 tween vegetation recovery and surface hydrology, as our models assume that  
1009 there are no feedbacks between these processes. Finally, D8 flow routing is

1010 probably not appropriate for post-MTR/VF summit flats, where extremely  
1011 low slopes are likely to cause diverging flow that requires a different ap-  
1012 proach (e.g., Tarboton, 1997). Flow routing can dramatically affect the pace  
1013 and style of landscape evolution (e.g., Lai and Anders, 2018); relaxing our  
1014 initial simplifying assumptions may improve future model predictions.

1015 Control simulations run from pre-MTR/VF DEMs should not be con-  
1016 strued as representing the dynamics of completely natural landscapes. Though  
1017 the pre-MTR/VF DEMs do pre-date widespread MTR/VF mining, they in-  
1018 corporate centuries of human disturbances to the Appalachian landscape  
1019 from logging to underground mining to bench-and-highwall contour mining,  
1020 all of which influence surface processes. While the pre- and post-mining com-  
1021 parison in our study allows us to elucidate how MTR/VF specifically affects  
1022 landscape evolution trajectories, and simulations run from pre-MTR/VF  
1023 DEMs provide the best approximation we have of how an equivalent undis-  
1024 turbed landscape might evolve, there are no truly undisturbed Appalachian  
1025 landscapes.

## 1026 **6. Conclusions**

1027 We leveraged an experiment in large-scale human landscape modification  
1028 to assess the influences of topography and vegetation on post-mining geo-  
1029 morphic change in MTR/VF-mined drainage basins. We first compared the  
1030 evolution of unmined versus mined topography under the assumption of no  
1031 vegetation change. We then incorporated the effects of post-mining revege-  
1032 tation by using gully mapping on mined landscapes to parameterize how the  
1033 erodibility of mined areas changes as a function of time since mining. We



1034 found that:

- 1035 1. When considering topographic effects alone, MTR/VF reduces total  
1036 sediment export because the creation of large summit flats outweighs  
1037 the effects of erosion hotspots on valley fill faces.
- 1038 2. If post-mining erodibility recovers 100% of the way to its pre-mining  
1039 state over 200 years, millennial sediment export from post-mining wa-  
1040 tersheds stays within the range of unmined watersheds.
- 1041 3. Conversely, if post-mining erodibility recovers less than 100% of the way  
1042 to its pre-mining states, millennial sediment export from post-mining  
1043 watersheds substantially exceeds that of unmined watersheds.
- 1044 4. Erosion is most rapid during the first few decades post-mining before  
1045 substantial vegetation recovery can occur, but the extent of vegetation  
1046 recovery also governs the 10 kyr—long beyond the recovery timescale—  
1047 trajectory of sediment fluxes from mined lands. A threshold exists  
1048 between 100% and 50% recovery that sets whether sediment fluxes  
1049 increase or decrease over time after recovery has ceased.
- 1050 5. Sediment export from mined lands is set by the integrated erodibility  
1051 over time, a function of how dramatic the disturbance in erodibility is,  
1052 how long it lasts, and the level to which it recovers.
- 1053 6. Erosion is concentrated on valley fill faces where artificial landforms  
1054 create slope–area disequilibrium, and along steep mine scarps.
- 1055 7. Deposition is greatest at the base of scarps and in low-order stream  
1056 valleys, where it has the potential to harm endangered aquatic species.

1057 Our results quantify the response of Appalachian landscapes to MTR/VF  
1058 mining over millennial timescales. Potential paths towards improved recla-

1059 mation outcomes emerge from our work. Over the short term, improving  
1060 erosion control during the first few decades post-mining when vegetation re-  
1061 covery is in its early stages can reduce sediment fluxes and the potential  
1062 for negative ecological effects like headwater stream sedimentation. Over  
1063 the long term, ensuring that vegetation is restored as closely as possible to  
1064 its pre-mining state can set sediment export on a downward trajectory over  
1065 time, and reducing the occurrence of dramatic slope–area disequilibrium can  
1066 prevent the formation of erosion hotspots. If the renewable energy transition  
1067 drives an increase in surface mining, drawing lessons from the past half-  
1068 century of MTR/VF mining will allow us to improve reclamation outcomes  
1069 and minimize disturbances to geomorphic and environmental systems.

## 1070 **Acknowledgements**

1071 The findings and conclusions in this publication are those of the authors  
1072 and should not be construed to represent any official USDA or U.S. Govern-  
1073 ment determination or policy. This work was supported by the NASA Estab-  
1074 lished Program to Stimulate Competitive Research, grant #80NSSC19M0054  
1075 (NASA West Virginia Space Grant Consortium). SJB was supported by a  
1076 Geological Society of America graduate student grant. We acknowledge time  
1077 on the West Virginia University Thorny Flat high-performance computing  
1078 cluster, which is supported by the NSF under MRI award #1726534. We  
1079 thank Leslie Hopkinson, Steve Kite, Rick Landenberger, and Miles Reed for  
1080 helpful discussions. Two anonymous reviewers improved the paper.

1081 **Data availability**

1082 All data not already publicly archived by agencies/researchers cited through-  
1083 out the paper, as well as code for analyses, are archived in Zenodo at  
1084 <https://dx.doi.org/10.5281/zenodo.10087618> (Bower and Shobe, 2023).

1085 **References**

1086 Barnes, R., 2017. Parallel non-divergent flow accumulation for trillion cell  
1087 digital elevation models on desktops or clusters. *Environmental Modelling*  
1088 & *Software* 92, 202–212.

1089 Barnhart, K.R., Hutton, E.W., Tucker, G.E., Gasparini, N.M., Istanbul-  
1090 luoglu, E., Hobley, D.E., Lyons, N.J., Mouchene, M., Nudurupati, S.S.,  
1091 Adams, J.M., et al., 2020a. Landlab v2. 0: a software package for earth  
1092 surface dynamics. *Earth Surface Dynamics* 8, 379–397.

1093 Barnhart, K.R., Tucker, G.E., Doty, S.G., Glade, R.C., Shobe, C.M., Rossi,  
1094 M.W., Hill, M.C., 2020b. Projections of landscape evolution on a 10,000  
1095 year timescale with assessment and partitioning of uncertainty sources.  
1096 *Journal of Geophysical Research: Earth Surface* 125, e2020JF005795.

1097 Barnhart, K.R., Tucker, G.E., Doty, S.G., Shobe, C.M., Glade, R.C.,  
1098 Rossi, M.W., Hill, M.C., 2020c. Inverting topography for landscape  
1099 evolution model process representation: 2. calibration and validation.  
1100 *Journal of Geophysical Research: Earth Surface* 125, e2018JF004963.  
1101 [doi:https://doi.org/10.1029/2018JF004963](https://doi.org/10.1029/2018JF004963).

- 1102 Bell, J.C., Daniels, W.L., Zipper, C.E., 1989. The practice of “approximate  
1103 original contour” in the central appalachians. i. slope stability and erosion  
1104 potential. *Landscape and Urban Planning* 18, 127–138.
- 1105 Bernhardt, E.S., Palmer, M.A., 2011. The environmental costs of moun-  
1106 taintop mining valley fill operations for aquatic ecosystems of the central  
1107 appalachians. *Annals of the New York Academy of Sciences* 1223, 39–57.
- 1108 Bower, S., Shobe, C., 2023. Code and data for: ”The  
1109 uncertain future of mountaintop-removal-mined landscapes  
1110 2: Modeling the influence of topography and vegeta-  
1111 tion”. URL: <https://doi.org/10.5281/zenodo.10087618>,  
1112 doi:10.5281/zenodo.10087618.
- 1113 Campforts, B., Shobe, C.M., Overeem, I., Tucker, G.E., 2022. The art of  
1114 landslides: How stochastic mass wasting shapes topography and influences  
1115 landscape dynamics. *Journal of Geophysical Research: Earth Surface* 127,  
1116 e2022JF006745.
- 1117 Coulthard, T.J., Skinner, C.J., 2016. The sensitivity of landscape evolution  
1118 models to spatial and temporal rainfall resolution. *Earth Surface Dynamics*  
1119 4, 757–771.
- 1120 Culling, W., 1963. Soil creep and the development of hillside slopes. *The*  
1121 *Journal of Geology* 71, 127–161.
- 1122 Dahinden, F., Fischer, E.M., Knutti, R., 2017. Future local climate unlike  
1123 currently observed anywhere. *Environmental Research Letters* 12, 084004.

- 1124 Davy, P., Lague, D., 2009. Fluvial erosion/transport equation of landscape  
1125 evolution models revisited. *Journal of Geophysical Research: Earth Sur-*  
1126 *face* 114.
- 1127 DeLisle, C., Yanites, B.J., 2023. Rethinking variability in bedrock rivers:  
1128 Sensitivity of hillslope sediment supply to precipitation events modulates  
1129 bedrock incision during floods. *Journal of Geophysical Research: Earth*  
1130 *Surface* , e2023JF007148.
- 1131 DePriest, N.C., Hopkinson, L.C., Quaranta, J.D., Michael, P.R.,  
1132 Ziemkiewicz, P.F., 2015. Geomorphic landform design alternatives for an  
1133 existing valley fill in central appalachia, usa: Quantifying the key issues.  
1134 *Ecological Engineering* 81, 19–29.
- 1135 Dethier, E.N., Renshaw, C.E., Magilligan, F.J., 2022. Rapid changes to  
1136 global river suspended sediment flux by humans. *Science* 376, 1447–1452.
- 1137 van Doorn, J., Ly, A., Marsman, M., Wagenmakers, E.J., 2020. Bayesian  
1138 rank-based hypothesis testing for the rank sum test, the signed rank test,  
1139 and spearman’s  $\rho$ . *Journal of Applied Statistics* 47, 2984–3006.
- 1140 Eaton, L.S., Morgan, B.A., Kochel, R.C., Howard, A.D., 2003. Role of debris  
1141 flows in long-term landscape denudation in the central appalachians of  
1142 virginia. *Geology* 31, 339–342.
- 1143 EPA, U., 2011. The effects of mountaintop mines and valley fills on aquatic  
1144 ecosystems of the central appalachian coalfields. Washington, DC .
- 1145 Evans, K., Willgoose, G., 2000. Post-mining landform evolution modelling:  
1146 2. effects of vegetation and surface ripping. *Earth Surface Processes and*

- 1147 Landforms: The Journal of the British Geomorphological Research Group  
1148 25, 803–823.
- 1149 Feng, Y., Wang, J., Bai, Z., Reading, L., 2019. Effects of surface coal mining  
1150 and land reclamation on soil properties: A review. *Earth-Science Reviews*  
1151 191, 12–25.
- 1152 Gallen, S.F., 2018. Lithologic controls on landscape dynamics and aquatic  
1153 species evolution in post-orogenic mountains. *Earth and Planetary Science*  
1154 *Letters* 493, 150–160.
- 1155 Greer, B.M., Burbey, T.J., Zipper, C.E., Hester, E.T., 2017. Electrical resis-  
1156 tivity imaging of hydrologic flow through surface coal mine valley fills with  
1157 comparison to other landforms. *Hydrological Processes* 31, 2244–2260.
- 1158 Guebert, M.D., Gardner, T.W., 2001. Macropore flow on a reclaimed surface  
1159 mine: infiltration and hillslope hydrology. *Geomorphology* 39, 151–169.
- 1160 Hancock, G., Duque, J.M., Willgoose, G., 2020a. Mining rehabilitation—using  
1161 geomorphology to engineer ecologically sustainable landscapes for highly  
1162 disturbed lands. *Ecological Engineering* 155, 105836.
- 1163 Hancock, G., Evans, K., Willgoose, G., Moliere, D., Saynor, M., Loch, R.,  
1164 2000. Medium-term erosion simulation of an abandoned mine site using  
1165 the siberia landscape evolution model. *Soil Research* 38, 249–264.
- 1166 Hancock, G., Loch, R., Willgoose, G., 2003. The design of post-mining land-  
1167 scapes using geomorphic principles. *Earth Surface Processes and Land-*  
1168 *forms: The Journal of the British Geomorphological Research Group* 28,  
1169 1097–1110.

- 1170 Hancock, G., Lowry, J., Coulthard, T., 2015. Catchment reconstruction—erosional stability at millennial time scales using landscape evolution  
1171 models. *Geomorphology* 231, 15–27.
- 1173 Hancock, G., Lowry, J., Coulthard, T., 2016. Long-term landscape trajectory—can we make predictions about landscape form and function for  
1174 post-mining landforms? *Geomorphology* 266, 121–132.
- 1176 Hancock, G., Saynor, M., Lowry, J., Erskine, W., 2020b. How to account for  
1177 particle size effects in a landscape evolution model when there is a wide  
1178 range of particle sizes. *Environmental Modelling & Software* 124, 104582.
- 1179 Hancock, G., Verdon-Kidd, D., Lowry, J., 2017a. Sediment output from a  
1180 post-mining catchment—centennial impacts using stochastically generated  
1181 rainfall. *Journal of Hydrology* 544, 180–194.
- 1182 Hancock, G., Verdon-Kidd, D., Lowry, J., 2017b. Soil erosion predictions  
1183 from a landscape evolution model—an assessment of a post-mining landform  
1184 using spatial climate change analogues. *Science of the Total Environment*  
1185 601, 109–121.
- 1186 Hancock, G.R., Willgoose, G.R., 2021. Predicting gully erosion using land-  
1187 form evolution models: Insights from mining landforms. *Earth Surface  
1188 Processes and Landforms* 46, 3271–3290.
- 1189 Hooke, R.L., 1999. Spatial distribution of human geomorphic activity in  
1190 the united states: comparison with rivers. *Earth Surface Processes and  
1191 Landforms: The Journal of the British Geomorphological Research Group*  
1192 24, 687–692.

- 1193 Hooke, R.L., 2000. On the history of humans as geomorphic agents. *Geology*  
1194 28, 843–846.
- 1195 Howard, A.D., Kerby, G., 1983. Channel changes in badlands. *Geological*  
1196 *Society of America Bulletin* 94, 739–752.
- 1197 Jaeger, K., Ross, M., 2021. Identifying geomorphic process domains in the  
1198 synthetic landscapes of west virginia, usa. *Journal of Geophysical Research:*  
1199 *Earth Surface* 126, e2020JF005851.
- 1200 Jaeger, K.L., 2015. Reach-scale geomorphic differences between headwater  
1201 streams draining mountaintop mined and unmined catchments. *Geomor-*  
1202 *phology* 236, 25–33.
- 1203 Kwang, J., Thaler, E., Larsen, I., 2023. The future of soils in the midwestern  
1204 united states. *Earth’s Future* 11, e2022EF003104.
- 1205 Lai, J., Anders, A.M., 2018. Modeled postglacial landscape evolution at the  
1206 southern margin of the laurentide ice sheet: Hydrological connection of  
1207 uplands controls the pace and style of fluvial network expansion. *Journal*  
1208 *of Geophysical Research: Earth Surface* 123, 967–984.
- 1209 Lowry, J., Coulthard, T., Hancock, G., 2013. Assessing the long-term geo-  
1210 morphic stability of a rehabilitated landform using the caesar-lisflood land-  
1211 scape evolution model, in: *Mine closure 2013: Proceedings of the eighth*  
1212 *international seminar on mine closure*, Australian Centre for Geomechan-  
1213 ics. pp. 611–624.



- 1214 Lowry, J., Narayan, M., Hancock, G., Evans, K., 2019. Understanding post-  
1215 mining landforms: Utilising pre-mine geomorphology to improve rehabili-  
1216 tation outcomes. *Geomorphology* 328, 93–107.
- 1217 Maxwell, A.E., Strager, M.P., 2013. Assessing landform alterations induced  
1218 by mountaintop mining. *Natural Science* 5, 229–237.
- 1219 Michael, P., Superfesky, M., Uranoswki, L., 2010. Challenges of applying  
1220 geomorphic and stream reclamation methodologies to mountaintop min-  
1221 ing and excess spoil fill construction in steep slope topography (eg central  
1222 appalachia), in: *Proceedings, Joint Conference of the 27th Annual Meet-*  
1223 *ings of the American Society of Mining and Reclamation, 12th Annual*  
1224 *Pennsylvania Abandoned Mine Reclamation Conference, and 4th Annual*  
1225 *Appalachian Regional Reforestation Initiative Mined Land Reforestation*  
1226 *Conference, ASMR, Lexington.* pp. 610–634.
- 1227 Miller, A.J., Zégre, N.P., 2014. Mountaintop removal mining and catchment  
1228 hydrology. *Water* 6, 472–499.
- 1229 Negley, T.L., Eshleman, K.N., 2006. Comparison of stormflow responses of  
1230 surface-mined and forested watersheds in the appalachian mountains, usa.  
1231 *Hydrological Processes: An International Journal* 20, 3467–3483.
- 1232 Nippgen, F., Ross, M.R., Bernhardt, E.S., McGlynn, B.L., 2017. Creating  
1233 a more perennial problem? mountaintop removal coal mining enhances  
1234 and sustains saline baseflows of appalachian watersheds. *Environmental*  
1235 *science & technology* 51, 8324–8334.

- 1236 Pearson, R.G., Stanton, J.C., Shoemaker, K.T., Aiello-Lammens, M.E., Er-  
1237 sts, P.J., Horning, N., Fordham, D.A., Raxworthy, C.J., Ryu, H.Y., Mc-  
1238 Nees, J., et al., 2014. Life history and spatial traits predict extinction risk  
1239 due to climate change. *Nature Climate Change* 4, 217–221.
- 1240 Pelletier, J.D., Brad Murray, A., Pierce, J.L., Bierman, P.R., Breshears,  
1241 D.D., Crosby, B.T., Ellis, M., Foufoula-Georgiou, E., Heimsath, A.M.,  
1242 Houser, C., et al., 2015. Forecasting the response of earth’s surface to  
1243 future climatic and land use changes: A review of methods and research  
1244 needs. *Earth’s Future* 3, 220–251.
- 1245 Pericak, A.A., Thomas, C.J., Kroodsmas, D.A., Wasson, M.F., Ross, M.R.,  
1246 Clinton, N.E., Campagna, D.J., Franklin, Y., Bernhardt, E.S., Amos, J.F.,  
1247 2018. Mapping the yearly extent of surface coal mining in central ap-  
1248 palachia using landsat and google earth engine. *PloS one* 13, e0197758.
- 1249 Phillips, J.D., 1997. Humans as geological agents and the question of scale.  
1250 *American Journal of Science* 297, 98–115.
- 1251 Phillips, J.D., 2004. Impacts of surface mine valley fills on headwater floods  
1252 in eastern kentucky. *Environmental Geology* 45, 367–380.
- 1253 Phillips, J.D., Van Dyke, C., 2016. Principles of geomorphic disturbance and  
1254 recovery in response to storms. *Earth Surface Processes and Landforms*  
1255 41, 971–979.
- 1256 Reed, M., Kite, S., 2020. Peripheral gully and landslide erosion on an extreme  
1257 anthropogenic landscape produced by mountaintop removal coal mining.  
1258 *Earth Surface Processes and Landforms* 45, 2078–2090.

- 1259 Richardson, P.W., Perron, J.T., Schurr, N.D., 2019. Influences of climate  
1260 and life on hillslope sediment transport. *Geology* 47, 423–426.
- 1261 Ross, M.R., McGlynn, B.L., Bernhardt, E.S., 2016. Deep impact: Effects of  
1262 mountaintop mining on surface topography, bedrock structure, and down-  
1263 stream waters. *Environmental science & technology* 50, 2064–2074.
- 1264 Ross, M.R., Nippgen, F., McGlynn, B.L., Thomas, C.J., Brooks, A.C.,  
1265 Shriver, R.K., Moore, E.M., Bernhardt, E.S., 2021. Mountaintop min-  
1266 ing legacies constrain ecological, hydrological and biogeochemical recovery  
1267 trajectories. *Environmental Research Letters* 16, 075004.
- 1268 Sears, A., Hopkinson, L., Quaranta, J., 2020. Predicting erosion at valley  
1269 fills with two reclamation techniques in mountainous terrain. *International*  
1270 *Journal of Mining, Reclamation and Environment* 34, 223–237.
- 1271 Shobe, C.M., 2022. How impervious are solar arrays? on the need for geomor-  
1272 phic assessment of energy transition technologies. *Earth Surface Processes*  
1273 *and Landforms* 47, 3219–3223.
- 1274 Shobe, C.M., Bower, S.J., Maxwell, A.E., Rachel, G.C., Samassi, N.M., in  
1275 review. The uncertain future of mountaintop-removal-mined landscapes 1:  
1276 How mining changes erosion processes and variables. *Geomorphology* .
- 1277 Shobe, C.M., Tucker, G.E., Barnhart, K.R., 2017. The space 1.0 model:  
1278 a landlab component for 2-d calculation of sediment transport, bedrock  
1279 erosion, and landscape evolution. *Geoscientific Model Development* 10,  
1280 4577–4604.

1281 Simon, A., Collison, A.J., 2002. Quantifying the mechanical and hydrologic  
1282 effects of riparian vegetation on streambank stability. *Earth surface pro-  
1283 cesses and landforms* 27, 527–546.

1284 Skousen, J., Zipper, C.E., 2014. Post-mining policies and practices in the  
1285 eastern usa coal region. *International journal of coal science & technology*  
1286 1, 135–151.

1287 Skousen, J., Zipper, C.E., 2021. Coal mining and reclamation in appalachia,  
1288 in: *Appalachia’s Coal-Mined Landscapes*. Springer, pp. 55–83.

1289 Sontter, L.J., Ali, S.H., Watson, J.E., 2018. Mining and biodiversity: key  
1290 issues and research needs in conservation science. *Proceedings of the Royal  
1291 Society B* 285, 20181926.

1292 Sovacool, B.K., Ali, S.H., Bazilian, M., Radley, B., Nemery, B., Okatz, J.,  
1293 Mulvaney, D., 2020. Sustainable minerals and metals for a low-carbon  
1294 future. *Science* 367, 30–33.

1295 Tarboton, D.G., 1997. A new method for the determination of flow directions  
1296 and upslope areas in grid digital elevation models. *Water resources research*  
1297 33, 309–319.

1298 Thomas, C.J., Shriver, R.K., Nippgen, F., Hepler, M., Ross, M.R., 2022.  
1299 Mines to forests? analyzing long-term recovery trends for surface coal  
1300 mines in central appalachia. *Restoration Ecology* , e13827.

1301 Tucker, G.E., 2009. Natural experiments in landscape evolution. *Earth  
1302 Surface Processes and Landforms* 34, 1450–1460.

- 1303 Tucker, G.E., Hancock, G.R., 2010. Modelling landscape evolution. *Earth*  
1304 *Surface Processes and Landforms* 35, 28–50.
- 1305 Vidal, O., Goffé, B., Arndt, N., 2013. Metals for a low-carbon society. *Nature*  
1306 *Geoscience* 6, 894–896.
- 1307 Wickham, J., Wood, P.B., Nicholson, M.C., Jenkins, W., Druckenbrod, D.,  
1308 Suter, G.W., Strager, M.P., Mazzarella, C., Galloway, W., Amos, J., 2013.  
1309 The overlooked terrestrial impacts of mountaintop mining. *BioScience* 63,  
1310 335–348.
- 1311 Wieczorek, G.F., Morgan, B.A., 2008. Debris-flow hazards within the Ap-  
1312 palachian Mountains of the Eastern United States. US Department of the  
1313 Interior, US Geological Survey.
- 1314 Wiley, J.B., 2001. Reconnaissance of stream geomorphology, low streamflow,  
1315 and stream temperature in the mountaintop coal-mining region, southern  
1316 West Virginia, 1999-2000. volume 1. US Department of the Interior, US  
1317 Geological Survey.
- 1318 Wilkinson, B.H., 2005. Humans as geologic agents: A deep-time perspective.  
1319 *Geology* 33, 161–164.
- 1320 Willgoose, G., Riley, S., 1998. The long-term stability of engineered land-  
1321 forms of the ranger uranium mine, northern territory, australia: applica-  
1322 tion of a catchment evolution model. *Earth Surface Processes and Land-*  
1323 *forms: The Journal of the British Geomorphological Group* 23, 237–259.
- 1324 Zipper, C.E., Burger, J.A., Skousen, J.G., Angel, P.N., Barton, C.D., Davis,

1325 V., Franklin, J.A., 2011. Restoring forests and associated ecosystem ser-  
1326 vices on appalachian coal surface mines. *Environmental management* 47,  
1327 751–765.

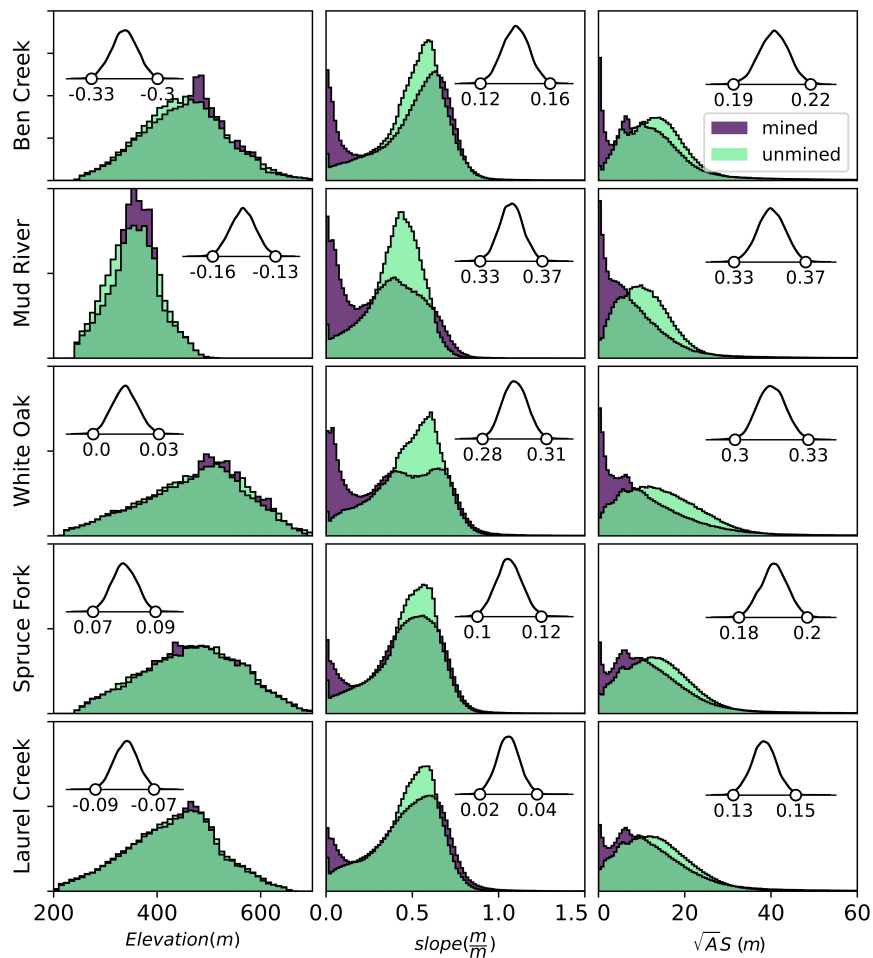


Figure 2: Differences in pre- and post-mining watershed topography. Histograms show counts of pixels in pre-mined and post-mined catchments. The inset density curve in each panel is the distribution of the test statistic from Bayesian Wilcoxon signed rank tests (van Doorn et al., 2020) comparing the two distributions. Points and labels mark the edges of the 99% highest posterior density interval (HPDI) for the posterior distribution of the test statistic. We consider the distributions to be significantly different if the 99% HPDI does not include zero.  $\sqrt{AS}$  is the slope-area product, a proxy for the efficacy of erosion by flowing water.

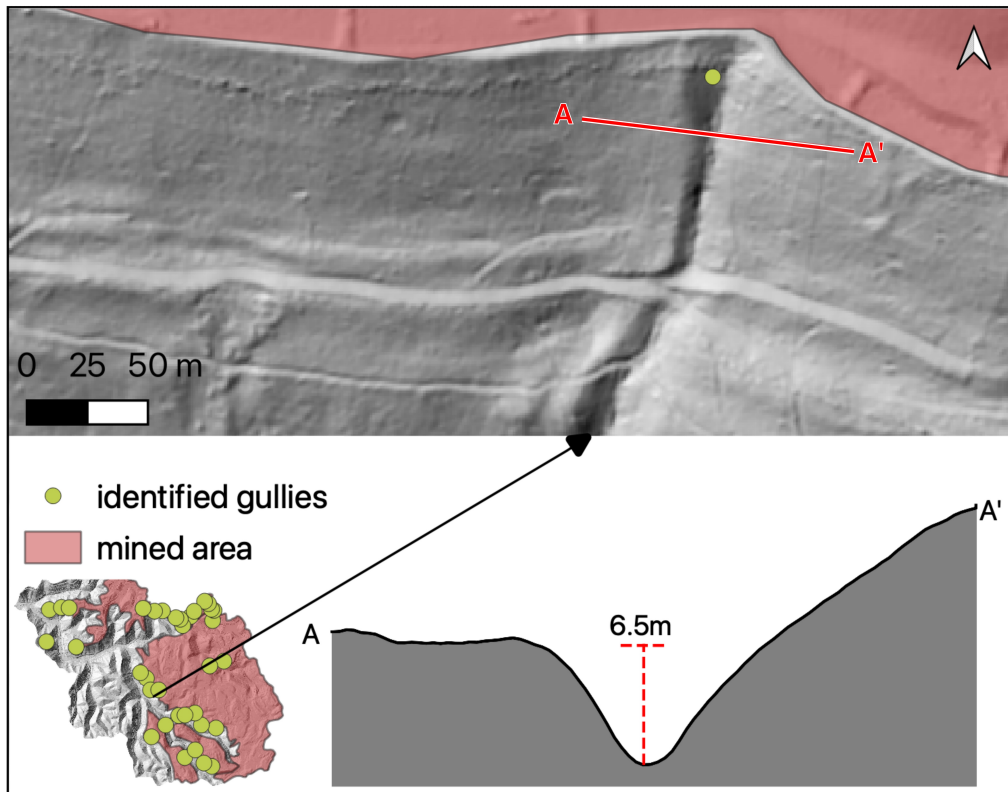


Figure 3: Lidar hillshade in the upper panel shows a gully identified on a peripheral hillslope in the White Oak watershed (approximate coordinates: 38.03 N, 81.51 W). This gully is representative of much of the fluvial incision occurring on mining-adjacent hillslopes (mined areas are red polygons). A cross section of the gully shows that it is approximately 6.5 m deep. All gully heads measured in the White Oak watershed are shown as green points in the catchment inset map.



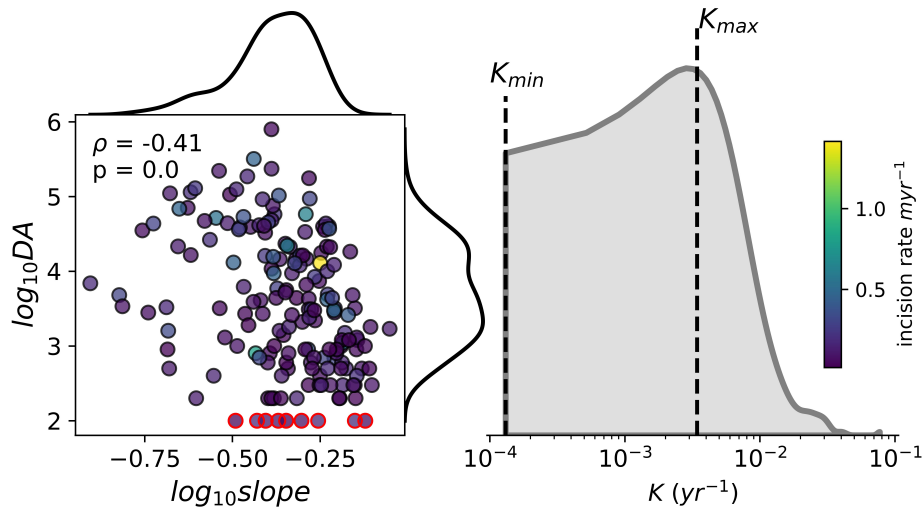


Figure 4: A) The slope, drainage area, and incision rate of each measured gully. A significant Spearman rank correlation suggests a monotonic relationship between slope and area, albeit with significant scatter. Red outlined points were excluded from the rank correlation and  $K$  calculations because they have  $A = 100 \text{ m}^2$ —these are DEM cells that drain only themselves. Such points arise from minor flow routing errors and are not representative of gully-forming drainage areas. B) The distribution of  $K$  calculated from erosion rate, slope and area. We take the median as the maximum  $K$  value we apply to mined portions of the landscape.

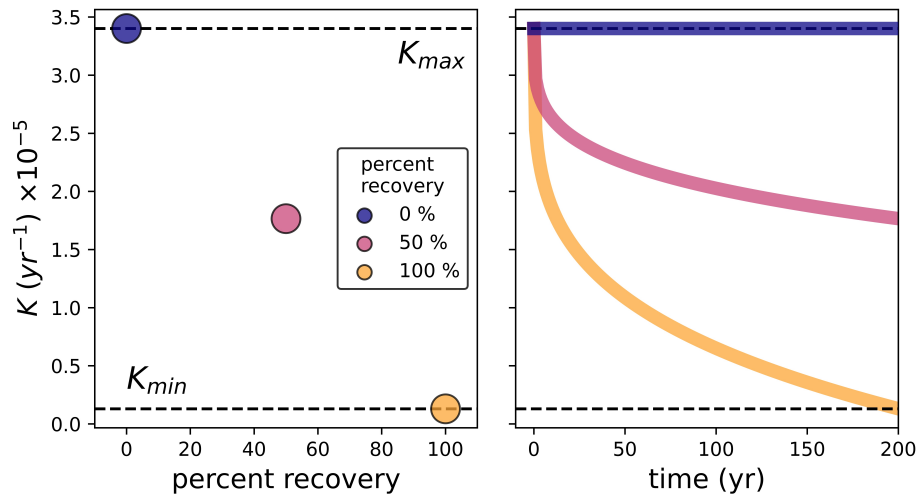


Figure 5: The three vegetation recovery scenarios. Each point represents a  $K_{min}^*$  value. Right panel shows a  $K$  recovery time series for each scenario, where each scenario begins at  $K_{max}$  and recovers towards the respective  $K_{min}^*$  shown in the left panel. From 200–10,000 years (i.e., the remainder of the simulation),  $K$  is held constant at its year 200 value.

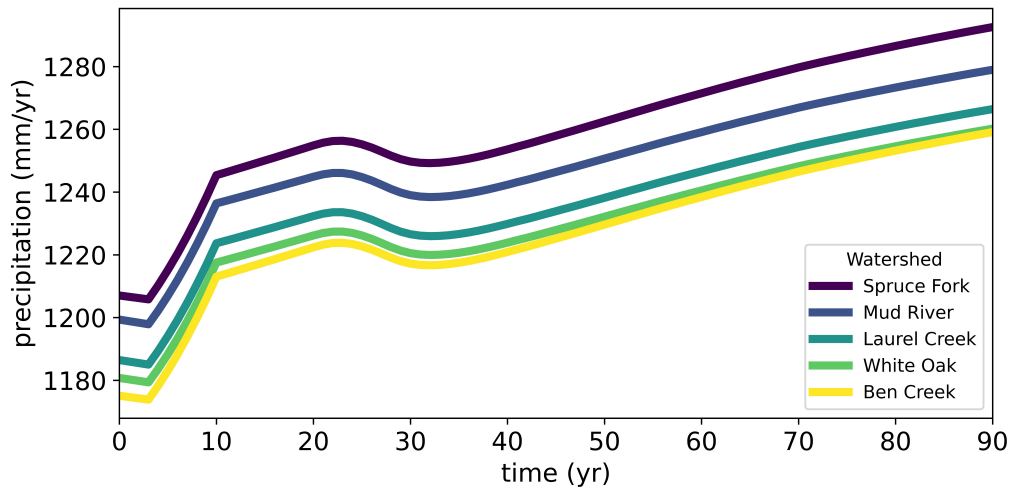


Figure 6: Mean annual precipitation projections from NASA's BioClim product (Pearson et al., 2014) averaged over each of the five study watersheds for the first 90 years of model time. Precipitation is held constant at its 90 year value after the first 90 years.

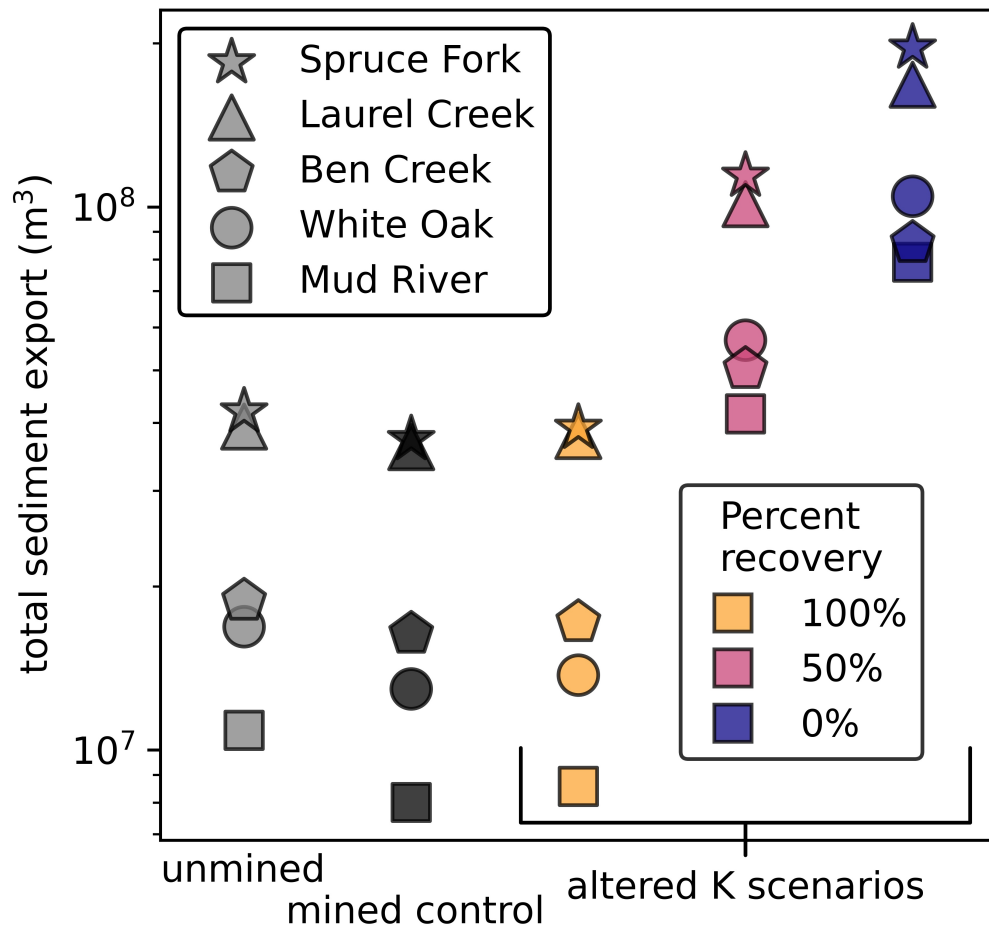


Figure 7: Total sediment export over 10 ky in each scenario. Unmined indicates simulations run using the pre-MTR/VF DEM with no changes in erodibility; mined control indicates simulations run using the post-MTR/VF DEM assuming no mining-induced changes in erodibility.

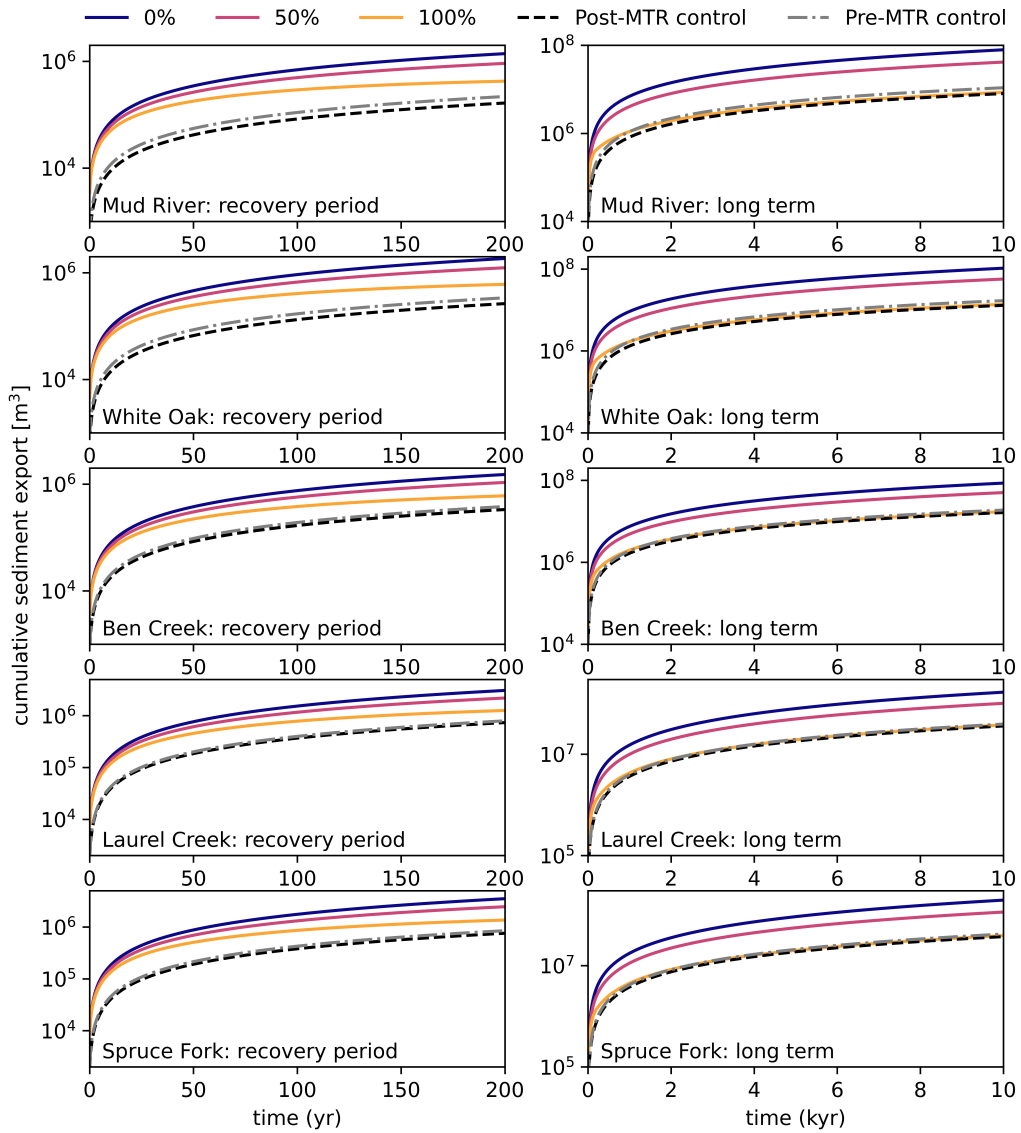


Figure 8: Cumulative sediment export for all five study watersheds over the first 200 years (the vegetation recovery period; left column) and the full 10 ky of model time (right column).

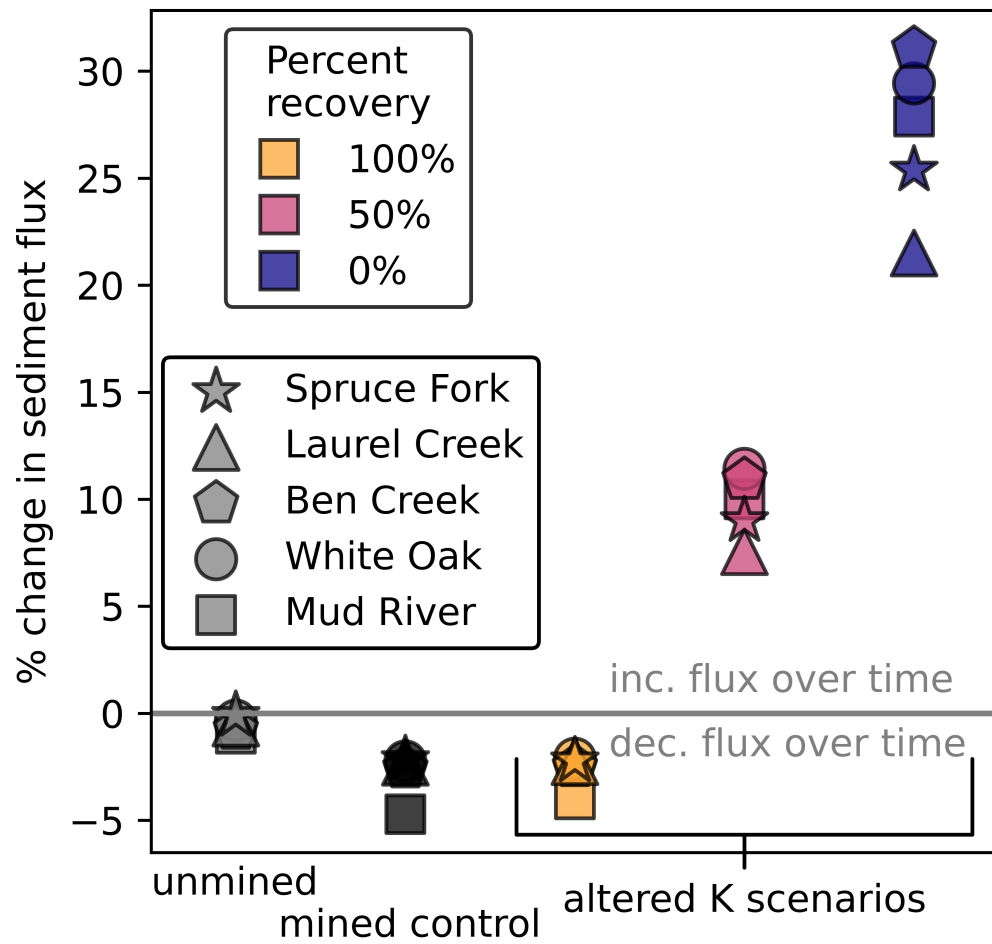


Figure 9: Percent change between sediment flux at year 200 and year 10,000. There exists a threshold between 100% and 50% recovery governing whether MTR/VF sets the landscape on a trajectory of increasing or decreasing sediment flux over time.

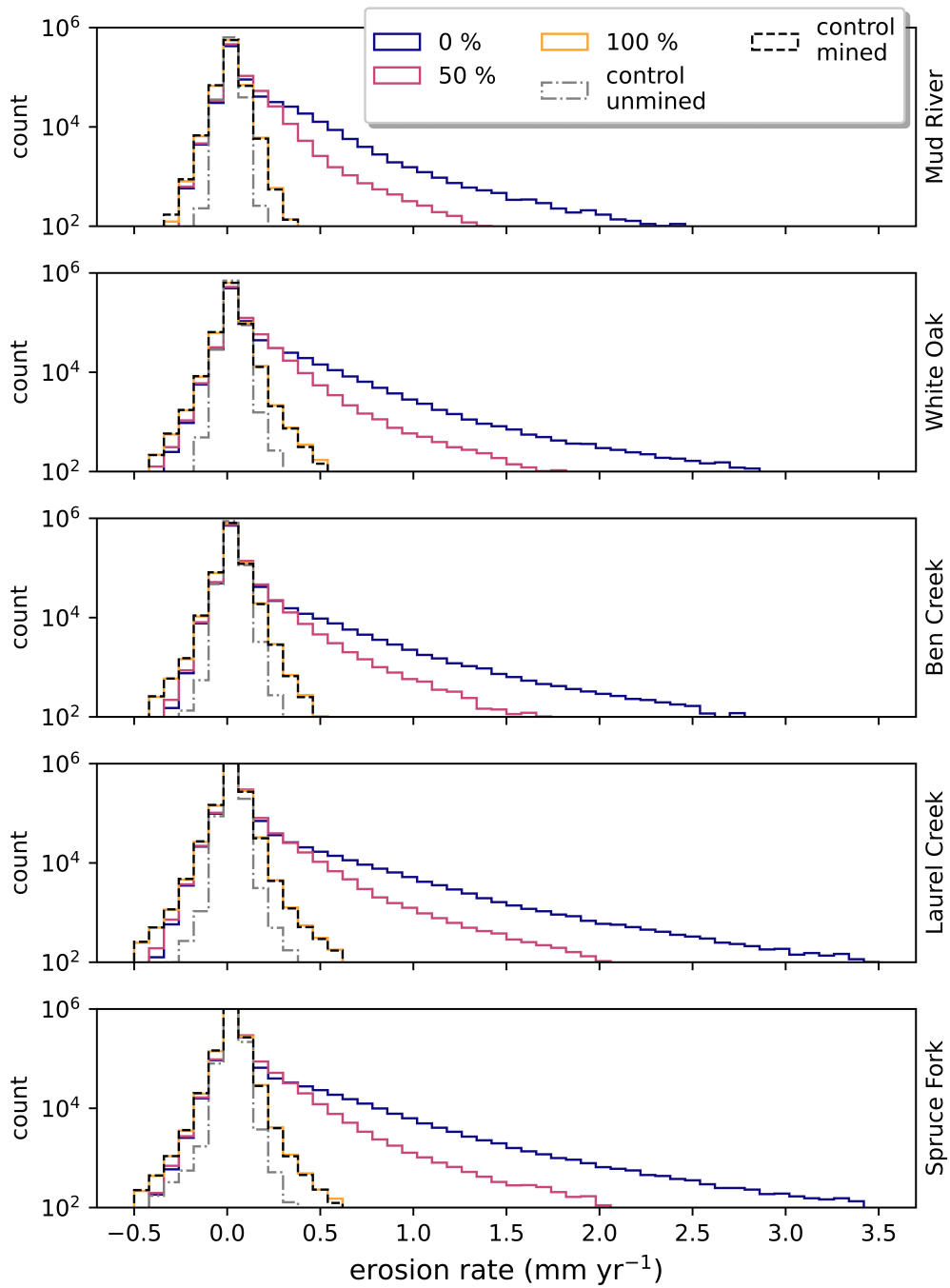


Figure 10: Distributions of erosion rates averaged over 10 kyr for all five catchments. Percentages refer to the vegetation recovery scenarios: 0%, 50%, or 100% recovery.

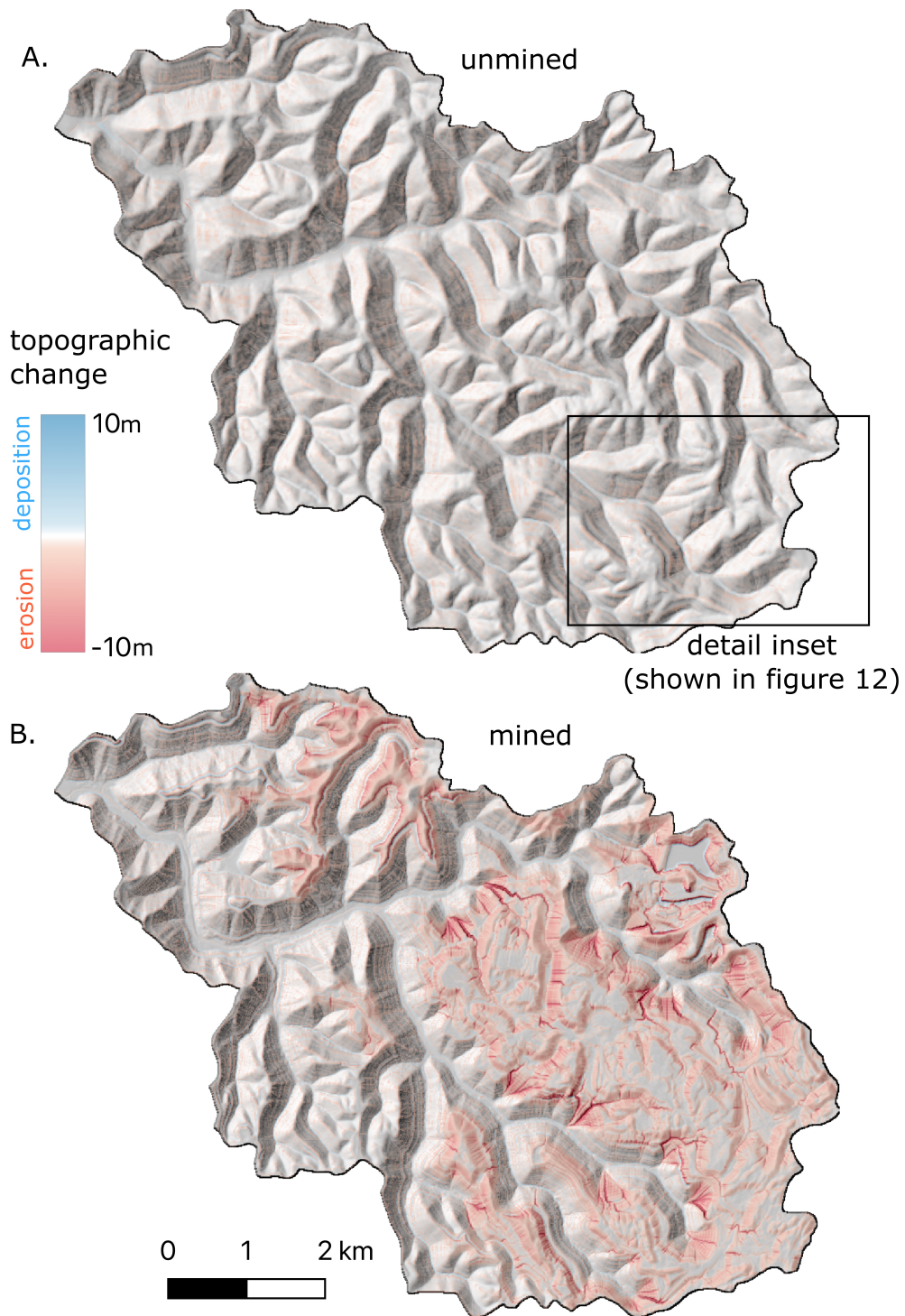


Figure 11: A) DEM of difference over 10 kyr from the White oak catchment for the 50% vegetation recovery scenario. Color bar is scaled for visual clarity; maximum erosion and deposition are -75.8 m and 7.4 m, respectively. Box shows extent of Fig. 12.



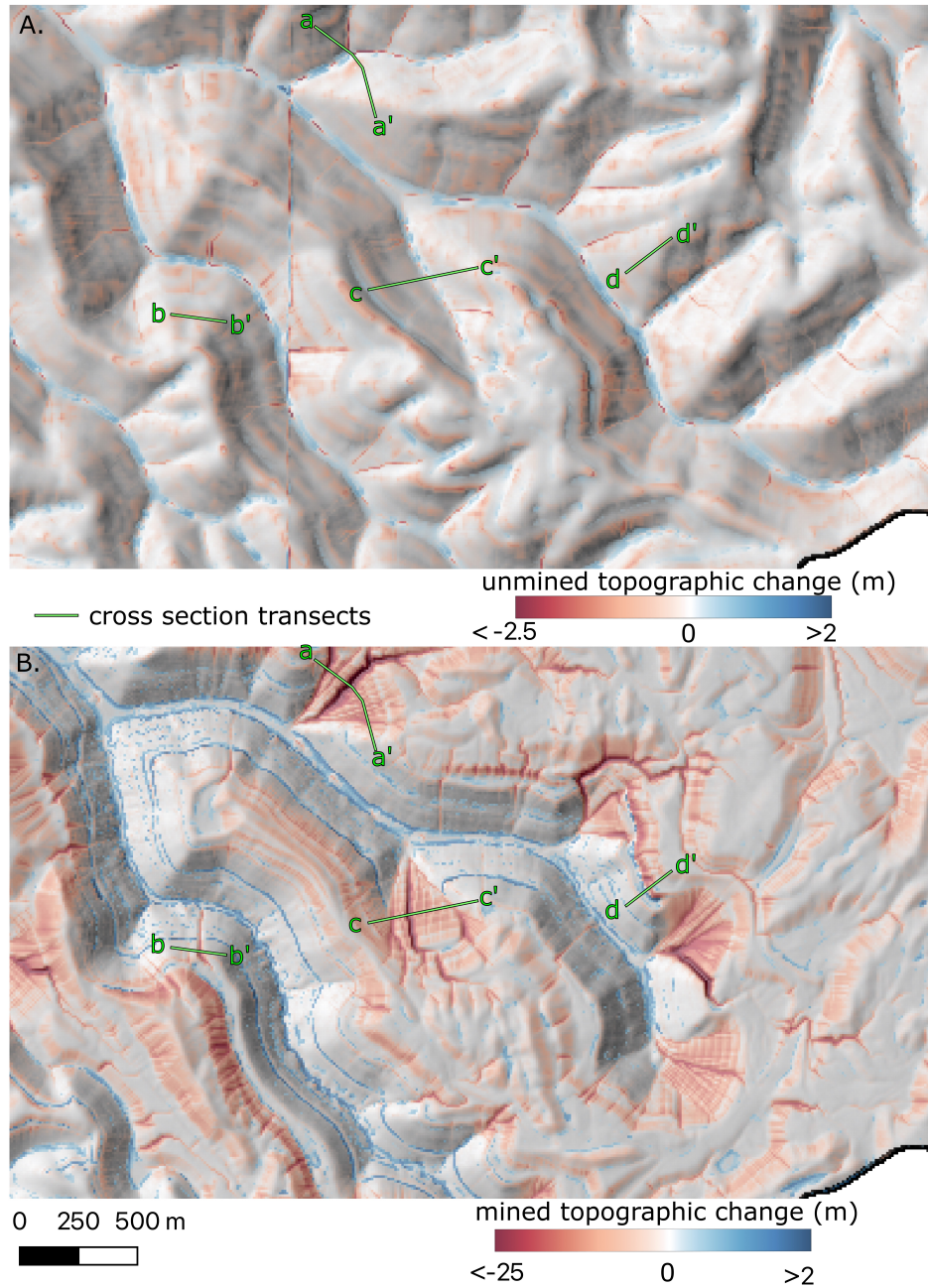


Figure 12: Selected comparisons between the unmined simulation (A) and the mined simulation with 50% vegetation recovery (B). Both panels share the same extent, shown by the bounding box in Fig. 11. Note that a different color scale is applied to each panel. The transects in each panel show the locations of cross-sections in Fig. 13. The along-contour banding in (A) reflects artefacts from the digitization of contour line topographic maps, resulting in spurious bands of predicted erosion. There is also a DEM mosaicing artefact in the center-left of (A).

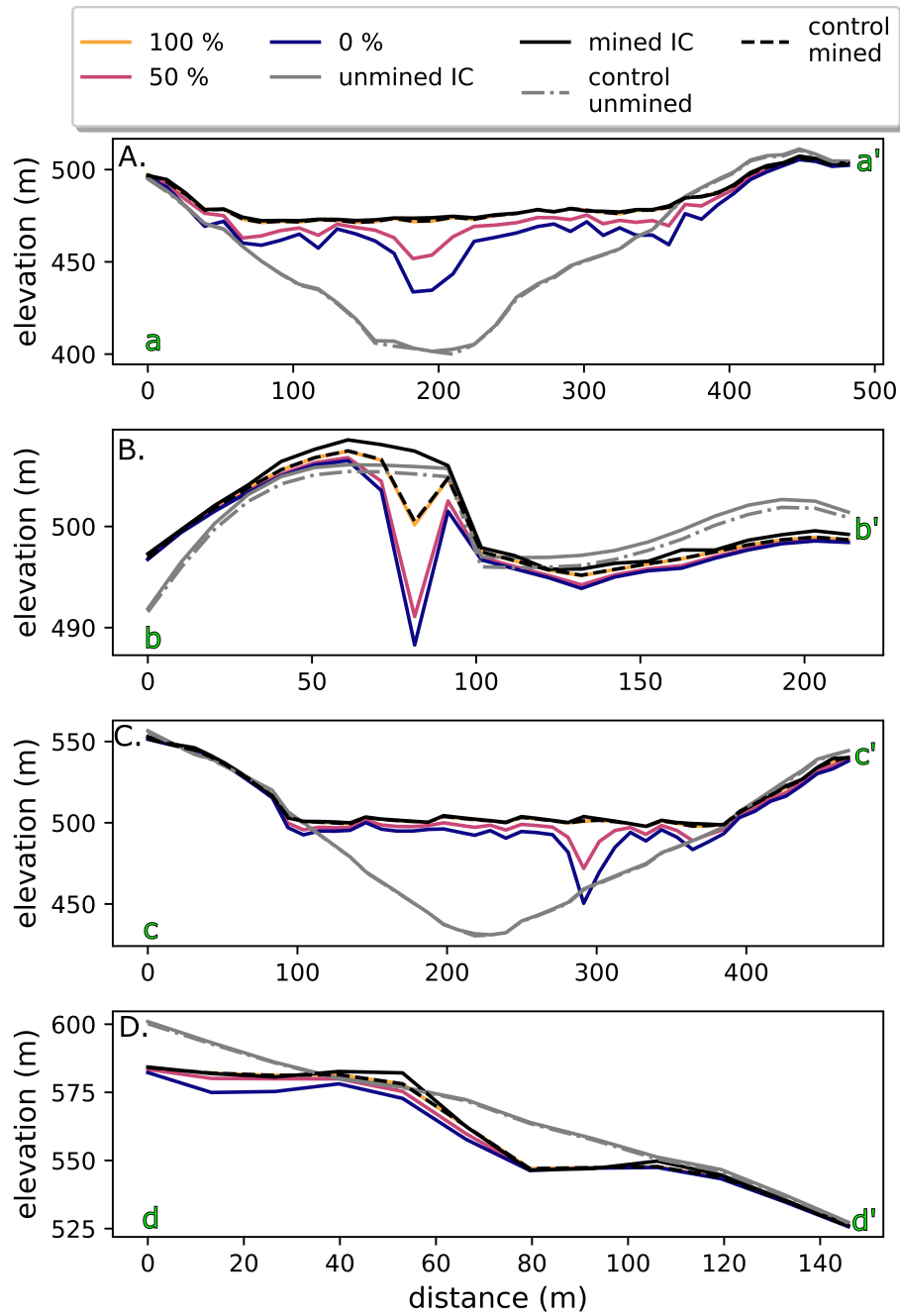


Figure 13: Evolution due to mining and subsequent post-mining erosion of cross sections corresponding to locations in Fig. 12. Cross-sections represent key landforms: A) and C) valley fill faces, B) mine-adjacent hillslope, and D) mine-related scarp.